Copyright © 1989, by the author(s).
All rights reserved.

Permission to make digital or hard copies of all or part of this work for personal or classroom use is granted without fee provided that copies are not made or distributed for profit or commercial advantage and that copies bear this notice and the full citation on the first page. To copy otherwise, to republish, to post on servers or to redistribute to lists, requires prior specific permission.

THE DYNAMIC RESPONSE OF A TACTILE SENSOR

by

Edward M. Sladek and Ronald S. Fearing

Memorandum No. UCB/ERL M89/138

6 December 1989

THE DYNAMIC RESPONSE OF A TACTILE SENSOR

by

Edward M. Sladek and Ronald S. Fearing

Memorandum No. UCB/ERL M89/138

6 December 1989

ELECTRONICS RESEARCH LABORATORY

College of Engineering
University of California, Berkeley
94720

TITLE PAGE

THE DYNAMIC RESPONSE OF A TACTILE SENSOR

by

Edward M. Sladek and Ronald S. Fearing

Memorandum No. UCB/ERL M89/138

6 December 1989

ELECTRONICS RESEARCH LABORATORY

College of Engineering
University of California, Berkeley
94720

The Dynamic Response of a Tactile Sensor

Edward M. Sladek
Ronald S. Fearing

Department of Electrical Engineering and Computer Science
Electronics Research Laboratory
University of California, Berkeley, CA 94720

Tactile sensing is important to Robotics for providing contact sensory information that can lead to improved grasping of objects, and aid in achieving dextrous manipulation. Because soft skin-like materials are generally viscoelastic, tactile sensors exhibit hysteresis. To be useful in a dextrous hand, this dynamic behavior of the sensor must be modeled and compensated for. A variety of tests were performed on a thumb shaped tactile sensor containing an eight by twenty array of tactile elements. Each element measures the strain of the rubber finger material at a certain point below the surface of the finger. To characterize the finger behavior, a precision force application device was designed. Static tests were performed to determine the steady state linearity of the elements with respect to force magnitude. The frequency response was determined in the range of 0.10 to 20 Hertz. Permanent deformation due to stress is seen to be predictable. The Maxwell-Kelvin model for viscoelasticity was fit to the stress-strain data obtained by probing the finger and recording the applied force and the strain response of a single element. Results show that the Maxwell-Kelvin model is better than a simple elastic model. A linear second order model was also fit to the stress-strain data. The model was inverted to predict the magnitude of the force of a point contact given the strain information of one tactile element. The second order inverse model predicted the force better than the elastic model.

The Dynamic Response of a Tactile Sensor

Edward M. Sladek
Ronald S. Fearing
Department of Electrical Engineering and Computer Science
Electronics Research Laboratory
University of California, Berkeley, CA 94720

1. Introduction: Viscoelastic Modeling of a Tactile Sensor

Tactile sensing is useful for shape interpretation and control of contact forces, Allen (1987), Dario and De Rossi (1985). It is one ingredient to achieving dextrous manipulation of objects for which there is little apriori information. Berkemeier and Fearing (1989) show that a finger tip shaped tactile sensor can be used to determine certain attributes of an object given a global class constraint. For example, after successfully grasping an object classified as a surface of revolution, only three tactile curvature measurements are needed to determine the direction of its axis and its location. Fearing and Hollerbach (1985) show that three strain measurements in an elastic material are sufficient to determine the location, magnitude, and direction of the force of a line contact. Both of these studies assume a steady state strain reading. In the process of grasping, however, a finger imparts time varying forces on the object being grasped and visa versa. Since most compliant materials, and thus tactile sensing fingers, tend to be viscoelastic, a model is needed to compensate for these viscoelastic affects. The intent is to process the strain data of a viscoelastic material so that the finger appears to be elastic. Time varying forces, permanent deformation from past stresses, and creep and relaxation dynamics, can make it difficult to interpret the tactile sensor data. This is the motivation for studying the viscoelastic behavior of a tactile sensor. Knowledge of this behavior will be used to develop schemes to estimate the magnitude of a point contact force at the surface of the finger given the strain response of one element of a tactile array.

The viscoelastic behavior of the rubber skin of the tactile sensor is reminiscent of human skin. Dinnar (1970) investigates the viscoelasticity of human skin. The strain of human tissue increases under constant stress and does not return quickly to its original dimensions. Nevertheless the human nervous system can still interpret and use tactile data.

A simple four parameter Maxwell-Kelvin model is investigated for the tactile sensor as was done for human tissue by Dinnar (1970). The model is fit to data obtained from several experiments. The data is obtained by measuring the force applied to the finger

and recording the strain response of a tactile element directly below the force probe. The strain of the tactile element is shown to be linear for loads of less than 35 grams and less linear as the load increases. This non-linear effect is incorporated into the Maxwell-Kelvin model, but no improvements based on the inclusion of nonlinear effects have been achieved. The Maxwell- Kelvin model predicted the finger response better than a simple elastic model. A general second order transfer function was also fit to the data, and its inverse was used to predict the forces at the surface of the finger.

Cutkosky and Howe (88) investigate dynamic tactile sensing by moving a sensor against an object and measuring the stress rate directly. Their experiments were focused on determining texture characteristics. Knowledge of texture is useful for grasping since it is related to the friction between a robotic finger and an object. They measure the current generated by piezo-electric film to obtain stress rate. Later, Cutkosky and Howe (89) used an accelerometer near the skin surface of a sensor to mimic the human ability to sense quick yet small displacements. Sensing this kind of motion could be useful for detecting the onset of slip and aid in maintaining a grasp. The consideration of viscoelastic effects was not necessary for their study since they were interested in directly measuring strain rate and strain acceleration, and not strain itself. The following treatment of dynamic tactile sensing refers to the study of the time and frequency domains of the strain of a tactile element that senses only strain and not strain rate or strain accelerations. Ideally a sensor would employ perhaps all three types of strain sensors.

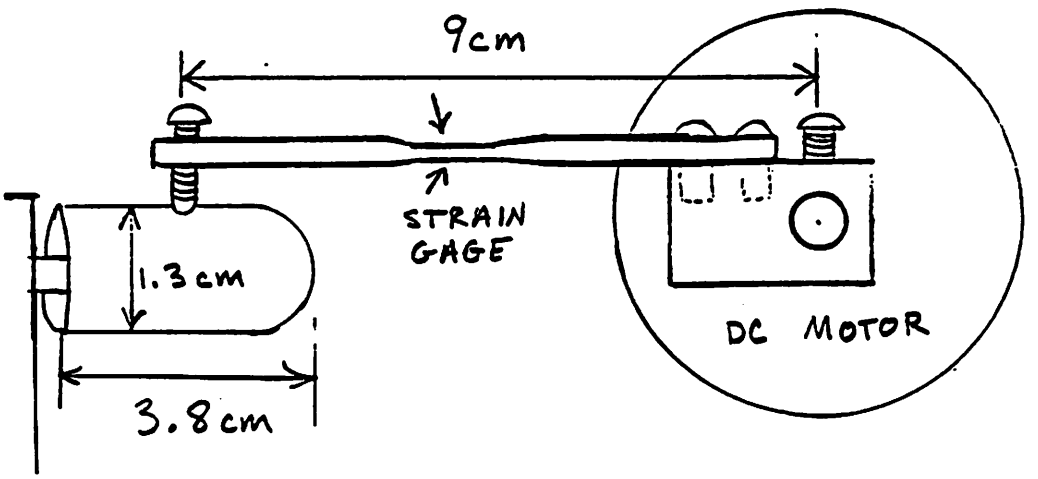

Figure 1. Force applicator system. The strain in the beam is controlled to provide a known contact force between the probe and finger.

The experiments were conducted using a motor-beam force applicator, see Figure 1. A control system using strain gage feedback from the aluminum beam was implemented and forces of up to 120 grams with a command error of +/– 1 gram can be applied (100 grams corresponds to 0.98 Newtons of force). The root-mean-square error of the noise of the strain gage signal was 0.14 grams. Stress is defined as force per unit area. The contact between the probe and the finger was hemispherical, having an area of 7 mm^2, so a 100 gram load is about $1.4 \times 10^5 N/m^2$ stress.

2. General Characteristics of the Tactile Sensor Being Studied

The tactile sensing finger used in this study was developed by Fearing (1987). It is cylindrical with a hemispherical tip, designed to be compatible with the Stanford/JPL hand. The finger contains an eight by twenty array of capacitors, which are the crossing points of conductive strips, see Figure 2. The capacitance is measured by applying a drive signal to one of the strips and measuring the voltage at one of the strips that crosses the drive strip. Each crossing point is one capacitive tactile element.

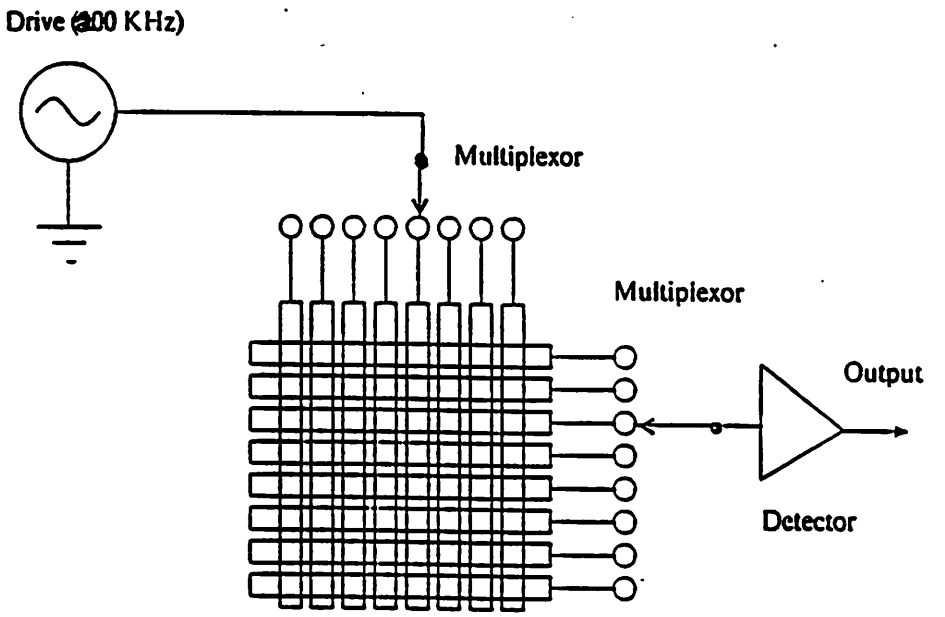

Figure 2. Diagram of the Array of Capacitive Tactile Elements. From Fearing (1987).

Figure 3 shows the two capacitor plates of an element pressed closer together by the deformation of the rubber. As the distance between the plates changes the capacitance changes, see equation (1). For a dielectric constant of 4 the capacitance is about 1 pF.

$$C = K_o \varepsilon_o \frac{A}{d_o - \Delta d} \tag{1}$$

C = capacitance of a tactile element

K_o = dielectric constant

ε_o = permittivity of free space

A = area = 2.5 *mm by* 5.1 *mm* = 12.75 mm^2

d_o = 0.7 *mm*

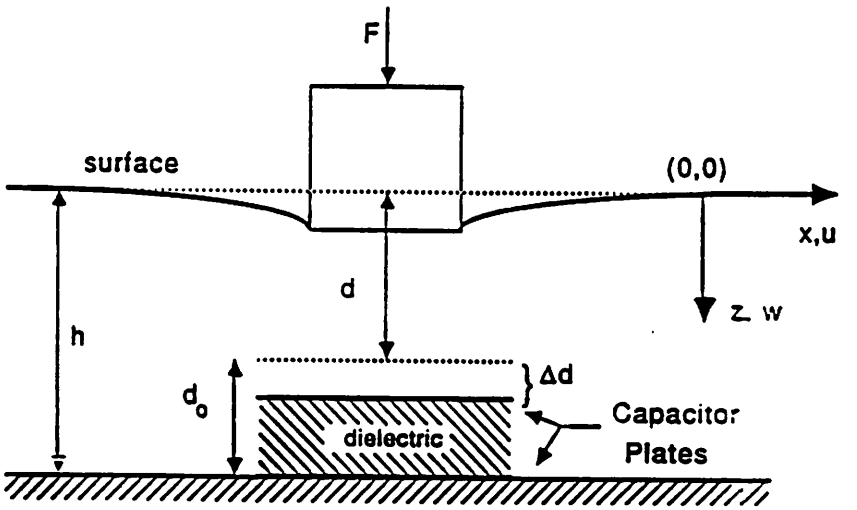

Figure 3. Strain of the rubber causes a change in the separation of capacitor plates. From Fearing (1987).

Figure 4 shows the capacitance of a tactile element shown in an electrical circuit. C_s designates the capacitance of the sensing element. C_l is a lumped capacitance that represents the capacitance between unselected strips, the cable capacitance, and the input capacitance of the amplifier. For very high frequencies with C_l much greater than the C_s, the subsurface strain can be nicely approximated by a measurable voltage, see equations (2) through (6). The voltage is amplified and processed to give the desired strain information.

$$|V_s| = \frac{|R_l \,//\, 1/j\omega C_l|}{|1/j\omega C_s + R_l \,//\, 1/j\omega C_l|} |V_d| = \frac{C_s R_l \omega}{\sqrt{1 + [\omega R_l (C_s + C_l)]^2}} |V_d| \tag{2}$$

C_s = capacitance of a tactile sensor element

C_l = capacitance of unselected elements, line capacitance and input capacitance of the amplifier lumped together

R_l = input resistance of amplifier

V_s = sensed voltage

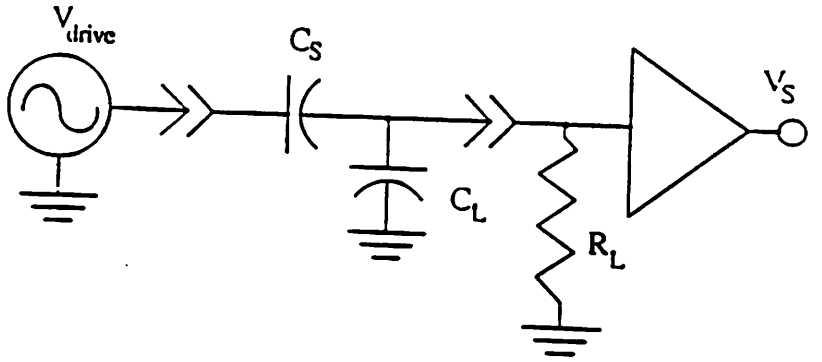

Figure 4. Tactile element capacitance, Cs, shown in the context of an electrical circuit.

V_d = drive voltage, 10 *volt* amplitude, 200 *kHz* sinewave
V_o = sensed voltage when there is no strain
ω = frequency of drive signal, $2\pi \times 200\ kHz$

for $C_l \gg C_s$ and large ω,

$$|V_s| \approx \frac{C_s R_l \omega}{\omega R_l C_l} |V_d| = \frac{C_s}{C_l} |V_d| \tag{3}$$

subsurface strain in the z direction,

$$\varepsilon_z = \frac{\Delta d}{d_o} \tag{4}$$

Relating voltages to capacitances and displacements using (3) and (1):

$$\frac{|V_s| - |V_o|}{|V_s|} = \frac{\frac{C_s}{C_l} - \frac{C_\infty}{C_l}}{\frac{C_s}{C_l}} = \frac{1/d - 1/d_o}{1/d} = \frac{d_o - d}{d_o} = \frac{\Delta d}{d_o} \tag{5}$$

Using (4) and (5) strain can be written as a function of measurable voltages:

$$\varepsilon_z = \frac{|V_s| - |V_o|}{|V_s|} \tag{6}$$

Figure 5a is a sketch of the inside of the finger. The finger is made up of a plastic (Delrin) core that supports twenty copper strips parallel to its axis. Surrounding the core and strips is a rubber mesh with seven copper strips that wrap around the core. A disk is put on the end of the cylindrical core for sensing at the tip of the finger. The rubber mesh is a dielectric to the capacitive tactile elements. The sensing array is covered by rubber for protection and force transmission.

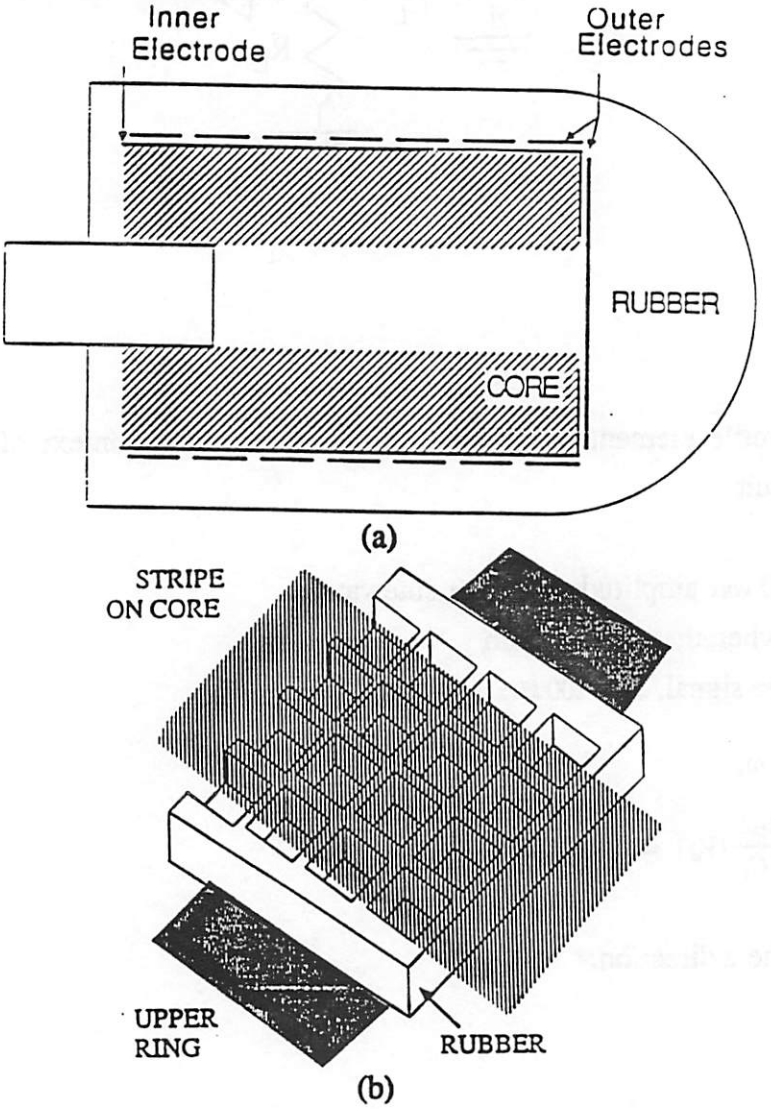

Figure 5. (a) Finger construction (b) the crossing points of the axial and radial electrodes are the capacitive tactile sensor elements. From Fearing (1987)

The capacitance between the axial and radial electrodes is sensed by applying a 20 volt peak to peak 200 kHz sinusoid to a radial electrode and sensing the voltage on an axial electrode. The resulting signal contains the strain information of the material at the crossing point of two electrodes. The sensed voltage is amplified and processed to give the percentage deflection of the rubber mesh dielectric. The experiments were conducted one element at a time, but other circuitry exists to time multiplex the information of an 8 by 8 array of tactile elements.

A static linearity test that was done by Fearing (1987) was repeated and Graph 1 (see graph section at end of paper) shows the results. For loads less than 35 grams the strain appears to be linearly related to the stress; however, as the load increases the percentage deflection does not increase linearly. For example, a 10 gram load yields a 1.8 % deflection, but a 70 gram load yields only a 1.5 % more deflection than does 60 grams. Note however, that in an operating range of plus or minus 10 grams about any point the strain vs. stress can be approximated by a straight line. The test was conducted using a 7 square mm hemispherical probe and applying loads up to 100 grams at 10 gram increments. The finger was allowed to rest for 19 seconds between loadings and a new finger offset was taken before applying the next load. One tenth of a second after the load was applied, the finger response was averaged over 10 samples separated by .001 seconds. This was done to measure the initial jump of the response instead of the delay or drift. The entire experiment was done five times and the result averaged. The x-axis shows the actual force applied as sensed by the strain gage on the force applicator beam. Graph 1b shows the same experiment for a larger, 16 square mm, flat force probe. The strain magnitude is not as great. This was to be expected since the same force over a larger area yields less pressure and thus less stress. Notice that the percent deflection does not fit a straight line at lesser loads. This has to do with the larger probe not approximating a point force as well as the smaller probe. This is significant since it emphasizes the fact that the strain of a single element is dependent on contact shape of a probe directly above the element. The following experiments and analysis were done with the smaller probe to approximate a point force more accurately.

The smaller probe experiment indicates that the strain becomes nonlinear at a smaller load than a different finger tested by Fearing (1987). The difference could be attributed to the use of a different set of amplifying electronics, but it will be shown later that the same set of electronics yields different model parameters for different elements. This discrepancy suggests that different fingers or different elements on the same finger can give slightly inconsistent results. To rectify this discrepancy, each element should be tested before use as a part of a calibration procedure. It is already known that the

sensitivity of various elements is not uniform, so the gain of each element needs to be calibrated. In addition to calibrating the static gain, a dynamic calibration would be advantageous.

The frequency response of the sensor shows a flat magnitude response from 0.1 to 20 Hertz, see Graph 2a. The phase lag, shown in Graph 2b, increases with frequency. Higher frequencies were not tested since the force stimulator does not track the desired input very well at frequencies greater than 20 Hz.

A sinewave with a slowly swept frequency was applied using the force stimulator. Graph 3 gives the impression that the magnitude of the frequency response of the sensor is flat up to 54 Hz. Note that the mean strain increases with time. This indicates that the viscoelastic drift of a step response superimposes with a sinusoid of exponentially increasing frequency. The flat response implies that there are no complicated dynamics in this frequency range.

The step response is more illuminative than the frequency response, since it shows three distinguishable attributes of a viscoelastic material. The strain response to a 50 gram step load is shown in Graph 4. Notice that the step response shows an initial jump, a constant drift and a delay that is apparently exponential. These characteristics provide the motivation for fitting the response to the Maxwell-Kelvin model for viscoelasticity (see section 3).

The most obvious characteristic is the initial, seemingly instantaneous jump of the strain response. Another effect of interest is the permanent deformation caused by an applied stress over time. The permanent deformation is shown in Graph 5. There was a 0.2 % residual deformation for a 50 gram load applied for 20 seconds, and roughly twice the residual deformation for a 100 gram load applied for 20 seconds. The consistency of the permanent deformation implies that it can be predicted.

One method for compensating for the deformation would be to take a new offset when no force is being applied. This approach has two disadvantages. First of all, the finger may be used to grasp an object for a several minutes, so that taking another offset may be inconvenient. Also, if the offset is retaken before the dynamic exponential factor has had a chance to decay, an erroneous offset would be obtained. Graph 6 shows the response to repeated 20 gram step loads. If the offset were taken even after 5 seconds of rest, an immediate error of 0.2 % deflection would occur.

3. The Maxwell-Kelvin Model of Viscoelasticity.

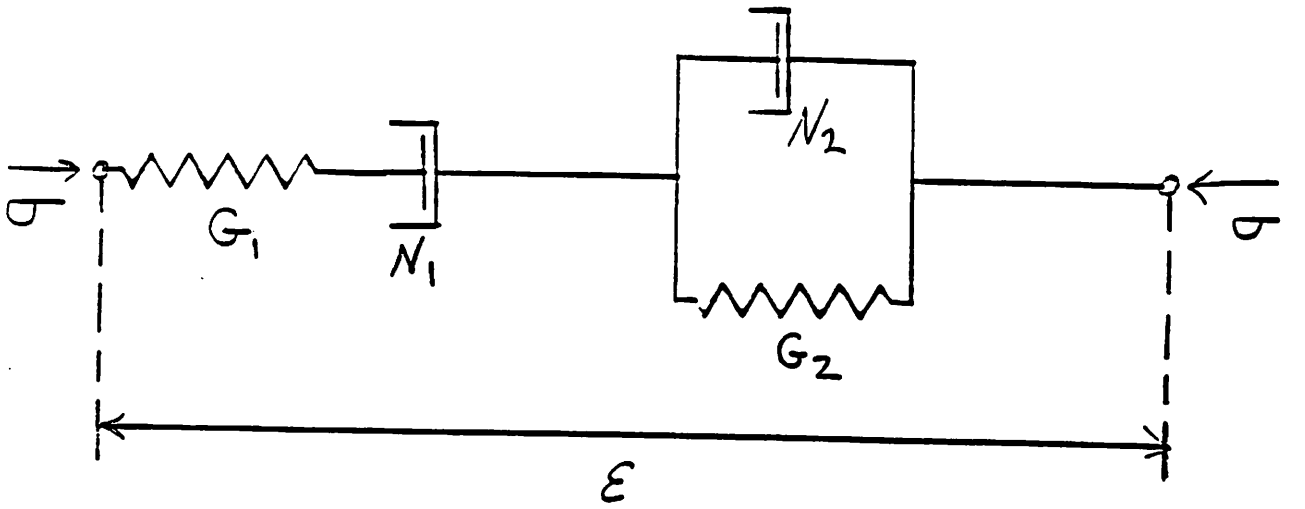

Figure 6. Maxwell-Kelvin Model of Viscoelasticity

The transfer function for the Maxwell-Kelvin model and its step response can be derived as done by Mase (1970). The model, shown in Figure 6, has two spring elements and two dashpot elements. Here the springs are ideally linear with their strain proportional to the stress applied. The dashpots represent a viscous response. The time rate of change of the strain of a dashpot is proportional to the stress applied. The first spring in series with a dashpot represents the Maxwell type response for a viscoelastic medium. The spring element reacts immediately to stress and the dashpot accounts for the drifting effect. Equations (7a) and (7b) give the relationships between strain, ε, and stress, σ, for the spring and the dashpot elements, respectively.

$$\varepsilon = \frac{\sigma}{G_1} \quad (a) \qquad \frac{d\varepsilon}{dt} = \frac{\sigma}{N_1} \quad (b) \tag{7ab}$$

G_1 = spring or elastic constant

N_1 = dashpot or viscous constant

Graph 7a shows the step response of a Maxwell medium. The strain response with respect to time for a step stress of σ_o is:

$$\varepsilon(t) = \frac{\sigma_o}{G_1} + \frac{\sigma_o}{N_1} t + \varepsilon_o \tag{8}$$

where ε_o = initial strain.

In series with the Maxwell model is a Kelvin model, which behaves as a common delay device. Its step response exhibits an exponential increase until it reaches a maximum strain level, see Graph 7b.

$$\varepsilon(t) = \frac{\sigma_o}{G_2}(1 - e^{-t\frac{G_2}{N_2}}) \tag{9}$$

The total strain for the two models in series is the sum of the individual strains. The stress on each section in series is the same. The state space equations for the single input single output, two state system are given by:

$$\begin{bmatrix} \dot{\varepsilon}_m \\ \dot{\varepsilon}_k \end{bmatrix} = \begin{bmatrix} 0 & 0 \\ 0 & G_2/N_2 \end{bmatrix} \begin{bmatrix} \varepsilon_m \\ \varepsilon_k \end{bmatrix} + \begin{bmatrix} 1/N_1 \\ 1/N_2 \end{bmatrix} \sigma \tag{10a}$$

$$\varepsilon = [1 \quad 1] \begin{bmatrix} \varepsilon_m \\ \varepsilon_k \end{bmatrix} + \frac{1}{G_1} \sigma \tag{10b}$$

where the dot denotes differentiation with respect to time and

ε_m = strain for dashpot of Maxwell part of the model

ε_k = strain for Kelvin section of the model

ε = total strain

σ = input stress.

Using the Laplace operator 's' to designate differentiation, the transfer function relating strain to stress is given below.

$$\frac{\varepsilon(s)}{\sigma(s)} = \frac{1}{G_1} + \frac{1}{sN_1} + \frac{1}{sN_2 + G_2} \tag{11}$$

Before implementing the Maxwell-Kelvin model for viscoelasticity it is wise to recognize its limitations. One significant consideration is the nonlinearity of the parameters of the model as seen in Graph 1. This is to be expected since the strain level is quite high, over 15 % deflection. This nonlinear effect reduces the validity of using a linear transfer function at all load levels, but near linearity suggests that a method of linearization about various operating points could be effective. Another problem is the consistency of the the model parameters for different tactile elements. Two tactile elements can differ considerably, as shown in Table III. It could be necessary to dynamically calibrate each sensor element of the tactile array. Also, the effects of age and work hardening can change the finger response so that the dynamic calibration may have to be done after a period of heavy use. An important problem with the Maxwell-Kelvin model is that it has a pole at the origin. This makes the model simulated response unstable. The instability is due to the fact that the model predicts that the strain will increase indefinitely as a constant stress is applied. This is certainly counter-intuitive since the material is of finite dimension. The reader should bear in mind that the accuracy of this type of model is valid only under the constraint that the loads on the finger do not last indefinitely. Also, stress from forces at other points on the finger can reverse the permanent deformation to put the tactile element back to its original position. Another consequence of the pole at the origin is that the inverse of the transfer function has a zero

at the origin. This makes it difficult to predict the stress given the strain by inverting the transfer function. This problem can be alleviated by a slight modification to the model that will follow in section 4.

Given the above problems with this model, it is still useful since it makes it easy to visualize the response contributed by each of the parameters of the model. It provides a basis for applying signal processing techniques that can be used to extract the contact forces from the finger strain data. A key advantage to this model is its simplicity.

The model is fit to four different step loads using a parameter identification tool called *maxlike* of the MATRIXx (trade mark of Integrated Systems Incorporated) system analysis software. Maxlike solves the optimization problem of minimizing the root mean square error, which is given in equation (12a). It uses the Armijo gradient decent method, Polak (1971), to find the optimal set of parameters, $G_1, N_1, N_2,$ and G_2. Another Matrixx tool called *lsim*, employs the Runge-Kutta-Merson algorithm, Ferziger (1981), to obtain the strain estimate of the entire signal based on the current parameter estimate. From the strain estimate the RMS error and the gradient of the RMS error can be calculated. The stress-strain data was in the form of 100 second trials sampled every 0.1 sec. For the purpose of comparison, the RMS error was normalized by dividing by the number of points of the signal and multiplying by the Maxwell spring term G_1 to yield error in grams instead of error in percentage deflection.

Root Mean Squared (RMS) Error:

$$RMS = \left[\sum_{i=1}^{N} (\hat{\varepsilon}_i - \varepsilon_i)^2 \right]^{1/2} \tag{12a}$$

N = number of points

Normalized root mean squared error converted to grams of error:

$$RMS_n = G_1 \left[\frac{\sum_{i=1}^{N} (\hat{\varepsilon}_i - \varepsilon_i)^2}{N} \right]^{1/2} \tag{12b}$$

The input for the estimation was a step load lasting for 50 seconds followed by a 25 second rest. The step load was chosen for illustrative purposes. The results are listed in Table I. The units for the spring terms, G_1 and G_2 are listed in grams per percentage deflection. This unit of measure is handy for examining the graphs (1 gram per percentage deflection for a 7 mm^2 probe is $1.4\times10^5 N/m^2$). The elastic constant for the 50 gram load experiment was $4.4\times1.4\times10^5 N/m^2 = 6.2 N/m^2$. This value is greater than the $2.5\times10^5 N/m^2$ reported by Fearing (1987) for an isolated sample of the rubber. The

additional stiffness can be attributed to the core. The units for the dashpot terms are in gram-seconds per percentage deflection (1 gram-second/percent deflection corresponds to $1.4\times10^5\ N-sec/m^2$). The value of the drift dashpot, N_1, was determined by calculating the slope of the response from 50 to 75 seconds, assuming that the exponential response had died out. Notice that the parameter values depend on the magnitude of the load. This was already seen for the immediate jump modeled by the spring of the Maxwell model (Graph 1 shows the elastic constant dependent on applied stress), and it appears to be true for the spring of the Kelvin model as well. The dashpot terms are more difficult to explain. The N_1 parameter can vary quite a bit, this is most likely due to experimental error, since its contribution is quite small. The amount of the contribution of the drift dashpot is only on the order of 1/6500 % deflection for each gram-second of load. It was seen previously that a 50 gram load for 20 seconds caused a 0.2% permanent deformation. This corresponds to a value of 5000 for N_1, quite close to the results of the parameter estimation here. The dashpot of the Kelvin model, N_2, has a reasonably consistent value of around 500.

Table I. Maxwell-Kelvin Model Parameters for Various Load Levels
Units for spring terms, G_1 and G_2, are *grams/%deflection*
Units for dashpot terms, N_1 and N_2, are *gram-seconds/%deflection*
Element 4,2 (4th ring from base, 2nd axial strip)

	10g	30g	50g	80g
G_1	2.4	3.6	4.4	5.3
N_1	5000	5770	6670	8250
N_2	500	500	500	300
G_2	26	47	66	90
Element 4,6				
G_1	4.3	4.8	5.1	5.7
N_1	7140	5000	6670	6560
N_2	500	500	500	500
G_2	48	65	70	75

Graph 8 shows the simulated response to the 50 gram step load for the Maxwell-Kelvin and elastic models. Table II shows a comparison between the Maxwell-Kelvin model and an elastic model for simulating the step response (Graph 4b) of finger element

4,6. The RMS error of the noise of the strain gage signal was 0.14 grams, and the RMS error of the noise of the finger signal was 0.022 grams. The strain gage noise was high, because its signal was amplified by 2100. The models were tuned using the step responses at various loads. The error for the Maxwell-Kelvin model was four times less than that of the elastic model for the 80g load. The error difference was greatest at the largest load. This is expected since the drift is proportional to stress, and the elastic model does not account for the drift.

Table II. Comparison of Maxwell-Kelvin Model and Elastic Model for Step Loads
Values are normalized root mean square error given in grams.
Element 4,6

	10g	30g	50g	80g
Maxwell-Kelvin	.204	.455	.474	.784
Elastic	.456	1.32	1.91	3.12

Graph 9 shows the error that arises when the 50 gram Maxwell-Kelvin parameters are used to predict the response of the 10 gram load. The most apparent discrepancy is the error in initial jump. After the load was removed at the 75 second mark the actual and predicted responses are quite close.

A true test of the model is to use it to predict the response of a random input. A pseudo-random input was created by arbitrarily selecting times for a step change in stress to occur. The step changes have random magnitudes, uniformly distributed from -20 grams to +20 grams. The best result came from using the parameters from the 30 gram model. This was to be expected since the input happened to be in the 20 to 40 gram range. Table III shows the error of simulating the pseudo-random response for each set of model parameters. Graph 10 compares the actual response with the response predicted by the model with the 30 gram parameters.

Table III. Simulation Error for Each Set of Model Parameters
Values are normalized root mean square error given in grams.
Element 4,2

10g Model 8.07
30g Model 2.33
50g Model 7.68
80g Model 14.44

4. General Second Order Transfer Function and Inversion

A general second order model can be derived by making a modification to the Maxwell-Kelvin model. Here the phrase "general second order model" means the transfer function of the model can be expressed as a ratio of two second order polynomials in 's', the Laplace operator. To arrive at the general second order model, the permanent deformation is modeled as an exponential delay with a very large time constant. This introduces a small spring value , α, in parallel with the first dashpot, see Figure 7.

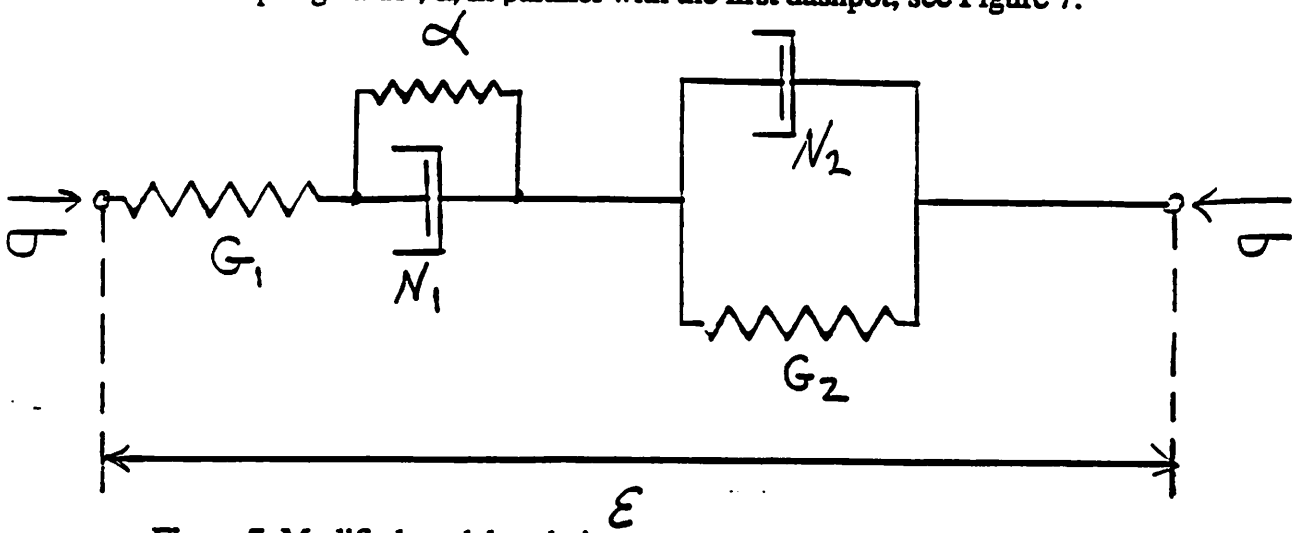

Figure 7. Modified model to derive a general 2nd order transfer function

This additional spring changes the transfer function as seen below.

Transfer function for modified model:

$$\frac{\varepsilon(s)}{\sigma(s)} = \frac{1}{G_1} + \frac{1}{sN_1+\alpha} + \frac{1}{sN_2+G_2} \tag{14}$$

Rearrange to obtain a ratio of polynomials:

$$= \frac{(N_1 s+\alpha)(sN_2+G_2) + G_1(sN_2+G_2) + G_1(sN_1+\alpha)}{G_1(sN_1+\alpha)(sN_2+G_2)} \tag{15}$$

$$= \frac{s^2N_1N_2 + s(N_1G_2+\alpha N_2+G_1N_2+G_1N_1) + (\alpha G_2+G_1G_2+G_1\alpha)}{s^2G_1N_1N_2 + s(G_1N_1G_2+G_1\alpha N_2) + G_1\alpha G_2} \tag{16}$$

$$= \frac{s^2+a_1s+a_2}{b_0s^2+b_1s+b_2} \tag{17}$$

The coefficients of the numerator and the denominator polynomials were determined by the Armijo gradient method as done before. The input excitation signal was the sum of 6 sinusoids having frequencies: 0.017, 0.23, 0.79, 0.062, 1.9, and 5 *Hz*. The offset load was 25 grams and the magnitude of each of the sinusoids was 4 grams. Each sinusoid was given a random phase shift. The results were...

$a_1 = 3.01 \quad a_2 = .784 \quad b_0 = 5.81 \quad b_1 = 13.26 \quad b_2 = 2.53$

error of 2nd order model predicting the excitation response = 2.78
error predicting random signal response = 3.71

Table IV. Pseudo-Random Signal Simulation
Values are normalized root mean square error given in grams.
Element 4,2

Elastic Model	4.54
Maxwell-Kelvin Model	3.85
2nd Order Model	3.71
Elastic Model Estimating Force	2.76
2nd Order Model Estimating Force	2.23

This model was used to estimate the finger response for the same pseudo-random signal as before. Table IV compares the results of the second order model with those of an elastic model and a Maxwell-Kelvin model tuned with the same excitation input. It is prudent to note that the Maxwell-Kelvin parameters converged to different values ($G_1 = 5.5$, $N_1 = 6000$, $N_2 = 19.2$, and $G_2 = 8.4$) for the estimation with the sum of sinusoids excitation signal. This is because the solution to the minimum error problem is not a unique point but rather a line or surface of points in 4-space. The estimator seemed to trade off between the values of the two spring terms. The reduction of G_2 brought down the value for N_2. This discrepancy is no cause for alarm, since the purpose of the model is to get a better prediction than an elastic model. This purpose is achieved as evidenced by the error comparisons and the graphs. The error of the elastic, Maxwell-Kelvin, and 2nd order models was less than the Maxwell-Kelvin models tuned with the 10g, 50g and 80g loads. This exemplifies the fact that the excitation signal needs to be in the load range of interest. Graph 11 compares the response of the second order model and response of the elastic model with the actual finger response for the pseudo-random input.

Next, the second order model was inverted by taking the reciprocal of its transfer function. This inverse was used to estimate the force of the contact point at the surface of the finger given the strain response of the tactile element. The error for the second order inverse simulation is also shown in Table IV and is roughly 20% less than the error of the elastic model. Graph 12 compares the inverse predicted force of the second order and elastic models with the actual force applied. Notice that the elastic model does not predict the zero force level well. This is because of the permanent deformation of the finger response. The second order model inverse overshoots for the initial jump up to 30 grams and undershoots at the final drop of 33 grams. The error caused by the undershoot can be reduced by limiting the predicted force to be greater than zero. This restriction is reasonable for this case since we are considering a normal force that can only press into the finger, and not grab the finger material and pull it up. A large part of the second order inverse force estimation error is due to the initial overshoot. This implies that instead of just taking the reciprocal of the transfer function, a more sophisticated method of force estimation based on the Maxwell-Kelvin model information may give better results.

5. Additional Considerations and Future Work

Based on the evidence that the spring terms of the Maxwell-Kelvin model are slightly nonlinear, a model that used look-up tables for the spring values was designed. The model was tested with the same pseudo- random input signal but no appreciable improvement was achieved. Other experiments were done to test the models.

For a different tactile element a second order model had greater success in simulating the response to a test signal comprised of consecutive 10 gram steps at one second intervals, see Graph 13. This experiment was conducted using the larger $16\,mm^2$ area probe. The RMS error was only 0.82 grams. The accuracy could be attributed to the fact that the steps were consistently increasing then decreasing. Also, this test lasted a total of only 10 seconds, so the exponential and permanent deformation effects did not play as significant a role as it did in the 100 second experiments.

The inverse of the second order model was taken as before. Graph 14 compares the actual force applied with the predicted force of the inverse model. The error was small because the overshoot problem did not contribute much error for the small 10 gram steps.

Incorporating hysteresis as a characteristic of the individual spring elements of the model is a conceivable approach for explaining the fact that the response does not return to zero when no force is applied. However, the step responses show that the immediate drop from unloading is of the same magnitude as the initial jump from loading. Hence,

hysteresis is not a characteristic of the individual spring elements.

6. Conclusion

The models presented here are not intended to be final models that can be immediately used to compensate for the viscoelasticity of the finger material. The contribution of this paper was to expose the viscoelastic characteristics of the sensor response and to suggest methods for dealing with these characteristics. The extent of modeling or signal processing of the sensor response will depend on the particular application of this tactile sensor.

Recovery of a dynamic point contact force has been aided by the consideration of viscoelastic effects. A second order linear transfer function can be inverted to yield better results than a strictly elastic model. Fitting a Maxwell-Kelvin model to the strain response of the finger demonstrates the model can simulate the finger strain of a pseudo-random input better than an elastic model. The error is only small when the parameters of any model are tuned with a signal in the same strain range as the test signal. The second order model had about 24 % less error than the elastic model for simulating the finger response to a pseudo-random signal. The majority of the error of the second order model came from the section of the signal that was outside an operating range of 25 to 30 grams of load. This implies that the reduction of error would be more dramatic if only the region near the operating range were considered. It is expected that some form of gain scheduling could compensate for the error caused by a widely varying strain signal. The viscoelastic drift is fairly consistent over various load levels at about 0.2 % deflection for a 1000 gram-second load. Hysteresis of the spring elements of the model is not the cause of permanent deformation. The frequency response is flat up to 20 Hz. A method of dynamic calibration of the tactile sensor elements needs to be employed in order to use viscoelastic modeling to an advantage. More work is needed in filtering the data to recover the contact forces, and an understanding of the effects of a dynamic shear stress at the surface of the sensor needs to be developed.

Acknowledgements: The authors would like to thank Raja Kadiyala for help with circuitry and software tools, Richard Murray for help with the LYMPH multiprocessor system, and John Hauser for control system and estimation advice. Supported in part by the Defense Advanced Research Projects Agency (DOD), monitored by SPAWAR under contract N00039-88-C-0292.

References

[1] Peter K. Allen, *Robot Object Recognition Using Vision and Touch*, Kluwer Academic Publishers, Boston, MA, 1987.

[2] Matthew D. Berkemeier and Ronald S. Fearing, "Determining the Axis of a Surface of Revolution Using Tactile Sensing", University of California, Berkeley/Electronics Reasearch Laboratory, ERL Memorandum no. UCB/ERL M89/117. 1989.

[3] Mark R. Cutkosky and Robert D. Howe, "Dynamic Tactile Sensing", *ROMANSY 88: Seventh CISM-IFToMM Symposium on the Theory and Practice of Robots and Manipulators*, Undine, Italy, September 12-15 1988.

[4] Mark R. Cutkosky and Robert D. Howe, "Sensing Skin Acceleration for Slip and Texture Perception", *IEEE Robotics & Automation Conference*, Vol. 1, pp 145-150. 1989.

[5] Paolo Dario and Danilo De Rossi, "Tactile Sensors and the Gripping Challenge", IEEE Spectrum 22(5):46-52, August 1985.

[6] Uri Dinnar, "A Note on the Theory of Deformation in Compressed Skin Tissues", *Mathematical Biosciences*, American Elsevier Publishing Company, Inc., 1970.

[7] Ronald S. Fearing, "Tactile Sensing, Perception and Shape Interpretation", Ph.D. Thesis, Stanford University, 1987.

[8] Ronald S. Fearing and John M. Hollerbach "Basic Solid Mechanics for Tactile Sensing", *The International Journal of Robotics Research*, Vol. 4, No. 3, Fall 1985.

[9] Joel H. Ferziger, *Numerical Methods for Engineering Application*, John Wiley & Sons, New York, NY, 1981

[10] M. S. Ghausi and K. R. Laker, *Modern Filter Design*, Prentice-Hall, Englewood Cliffs, NJ, 1981.

[11] J. N. Goodier and S. Timoshenko, *Theory of Elasticity*, Mc Graw-Hill Book Company, New York, NY, 1951.

[12] Graham C. Goodwin and Kwai Sang Sin, *Adaptive Filtering Prediction and Control*, Prentice-Hall, Inc., Englewood Cliffs, NJ 1984.

[13] John M. Hollerbach, "Tactile Sensors and the Interpretation of Contact Features", *Workshop on Intelligent Robots: Issues and Achievements*, pages 143-152, SRI International, Menlo Park, CA, November 13-14, 1984.

[14] K. L. Johnson, *Contact Mechanics*, Cambridge University Press, Cambridge, NY, 1987.

[15] P.R. Kumar and Pravin Varaiya, *Stochastic Systems: Estimation, Identification, and Adaptive Control*, Prentice-Hall, Inc., Englewood Cliffs, NJ, 1986.

[16] George E. Mase, *Schaum's Outline of Theory and Problems of Continuum Mechanics*, Mc Graw-Hill Book Company, New York, NY, 1970.

[17] Thomas J. Moore "A Survey of the Mechanical Characteristics of Skin and Tissue in Response to Vibratory Stimulation", *Transactions on Man-Machine Systems*, Vol. M MS-11, No. 1 March 1970.

[18] Alan V. Oppenheim and Alan S. Willsky, *Signals & Systems*, Prentice-Hall, Inc., Englewood Cliffs, NJ, 1983.

[19] E. Polak, *Computational Methods in Optimization*, Academic Press, Inc. Orlando, FL. 1971.

[20] Francis Sears, Hugh Young, and Mark Zemansky, *University Physics*, Addison-Wesley Publishing Company, Reading, MA, 1977.

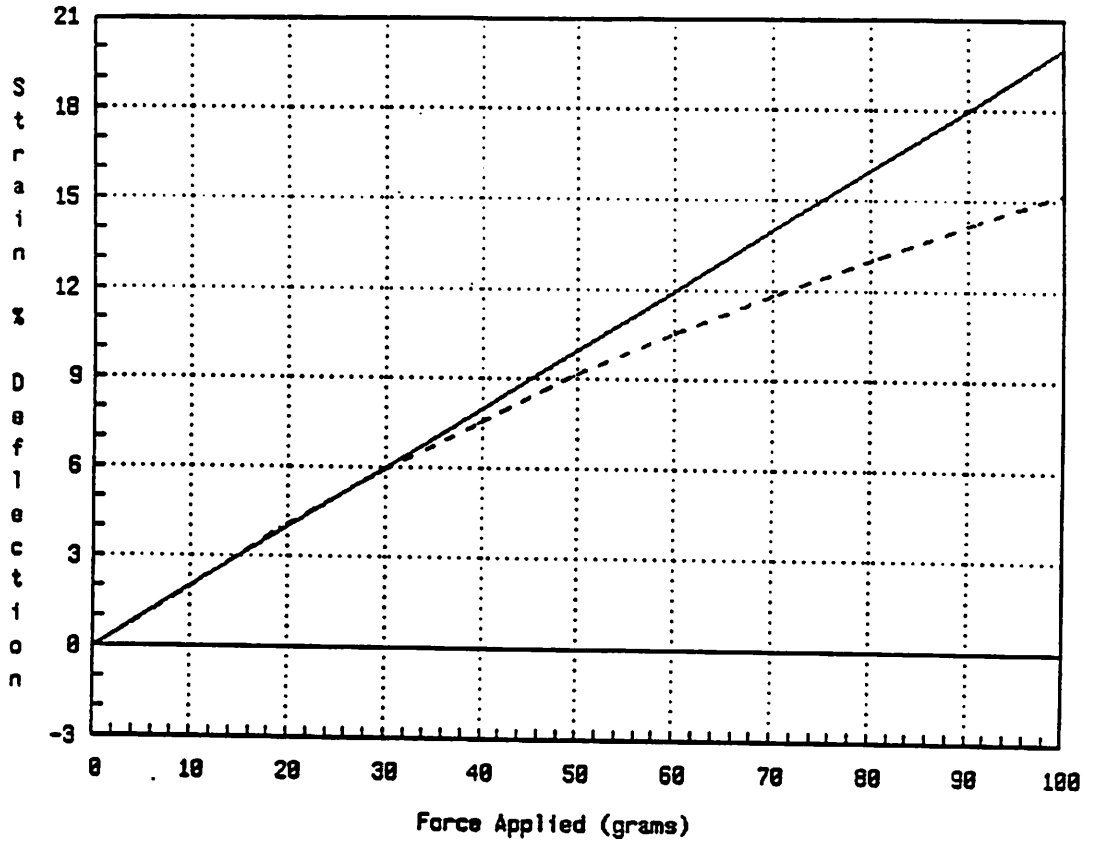

(a)

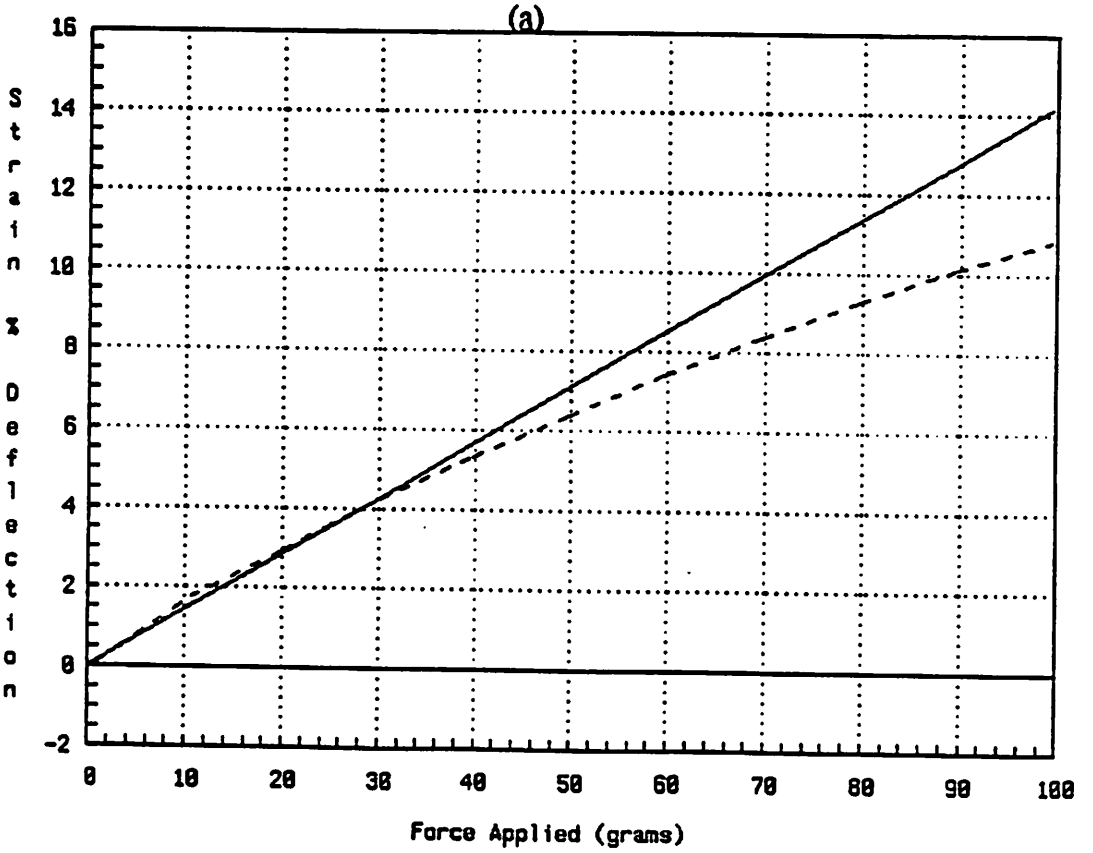

(b)

Graph 1. Static linearity test, finger response taken 0.1 sec after each load was applied. (a) $7mm^2$ area probe (b) $16mm^2$ area probe

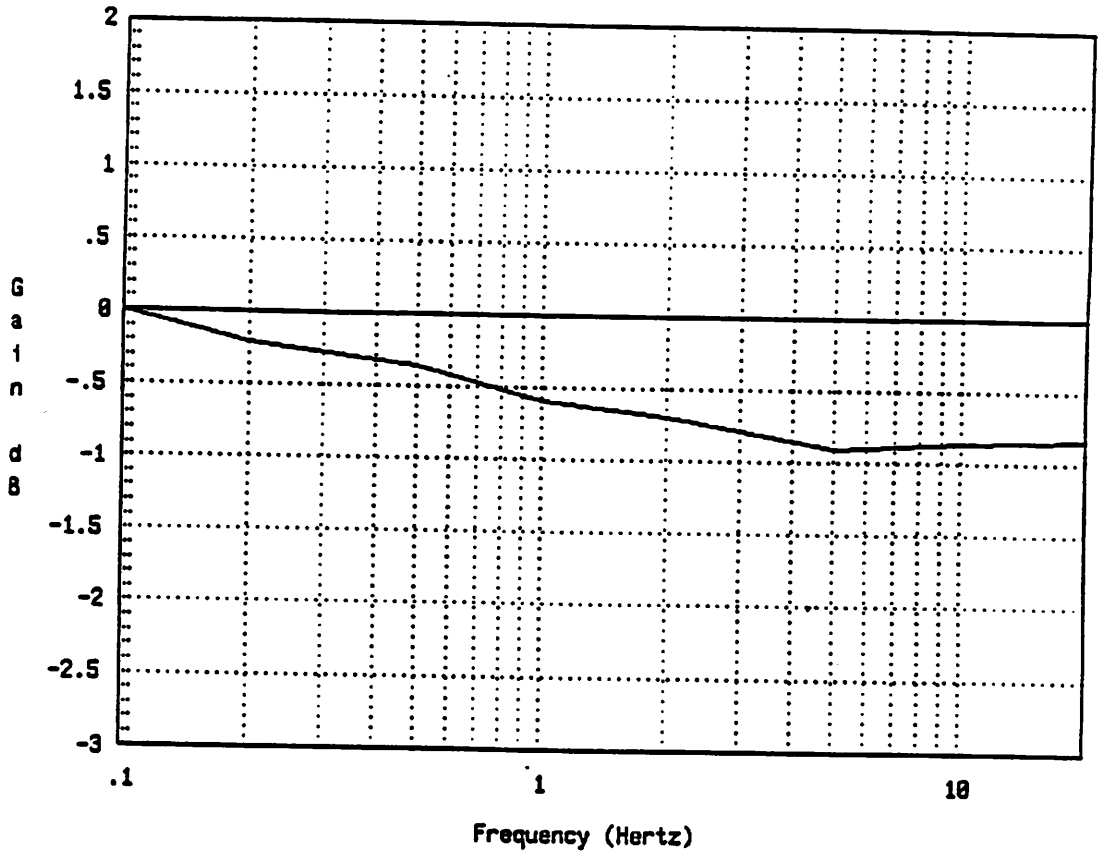

(a)

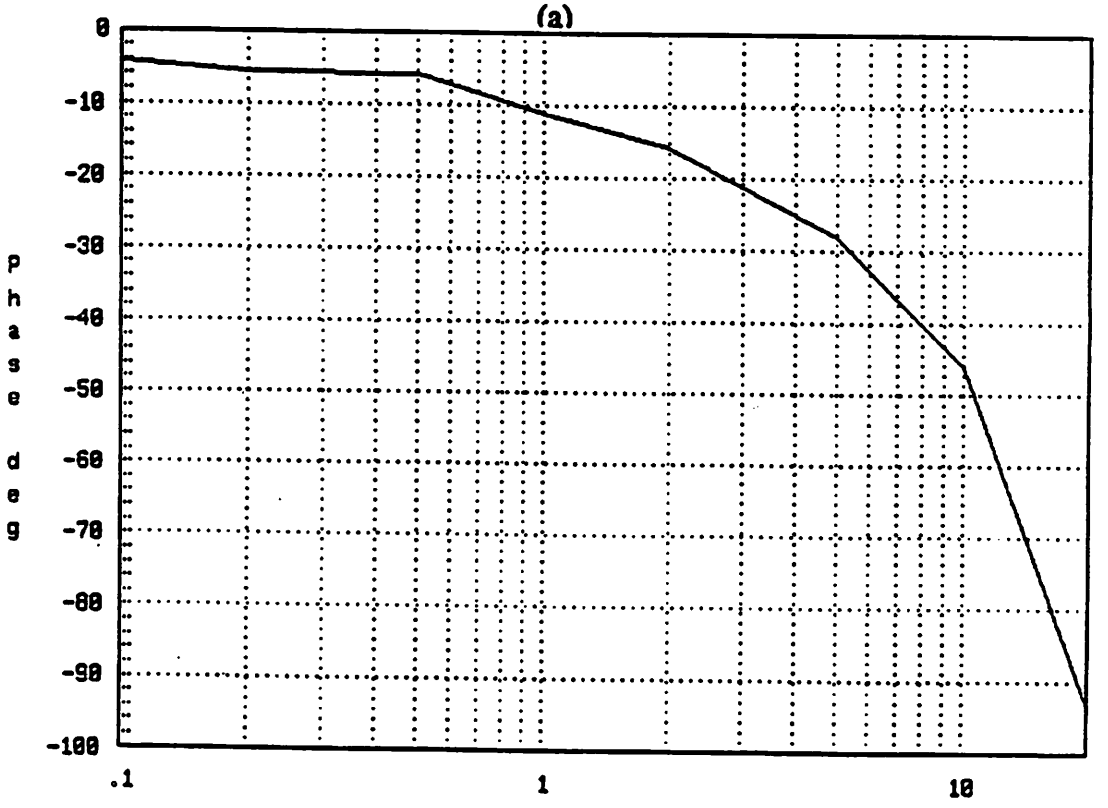

(b)

Graph 2. Frequency response of a tactile element. (a) magnitude reponse (b) phase response

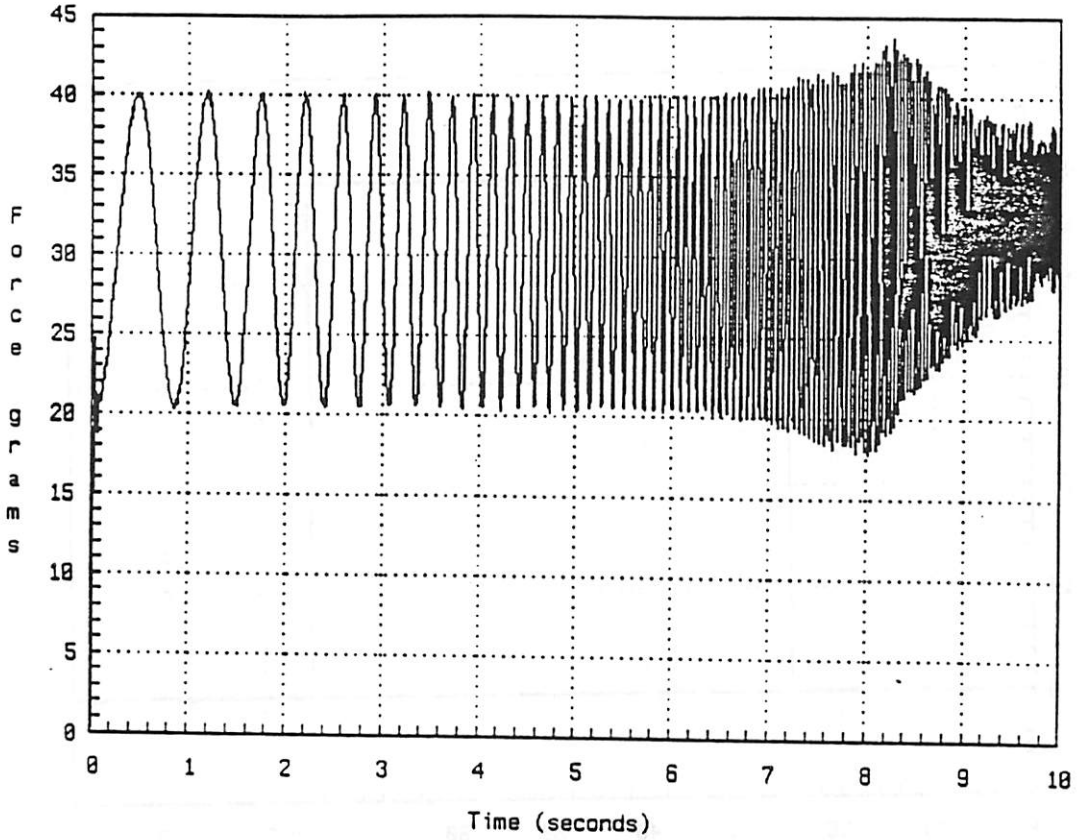

(a)

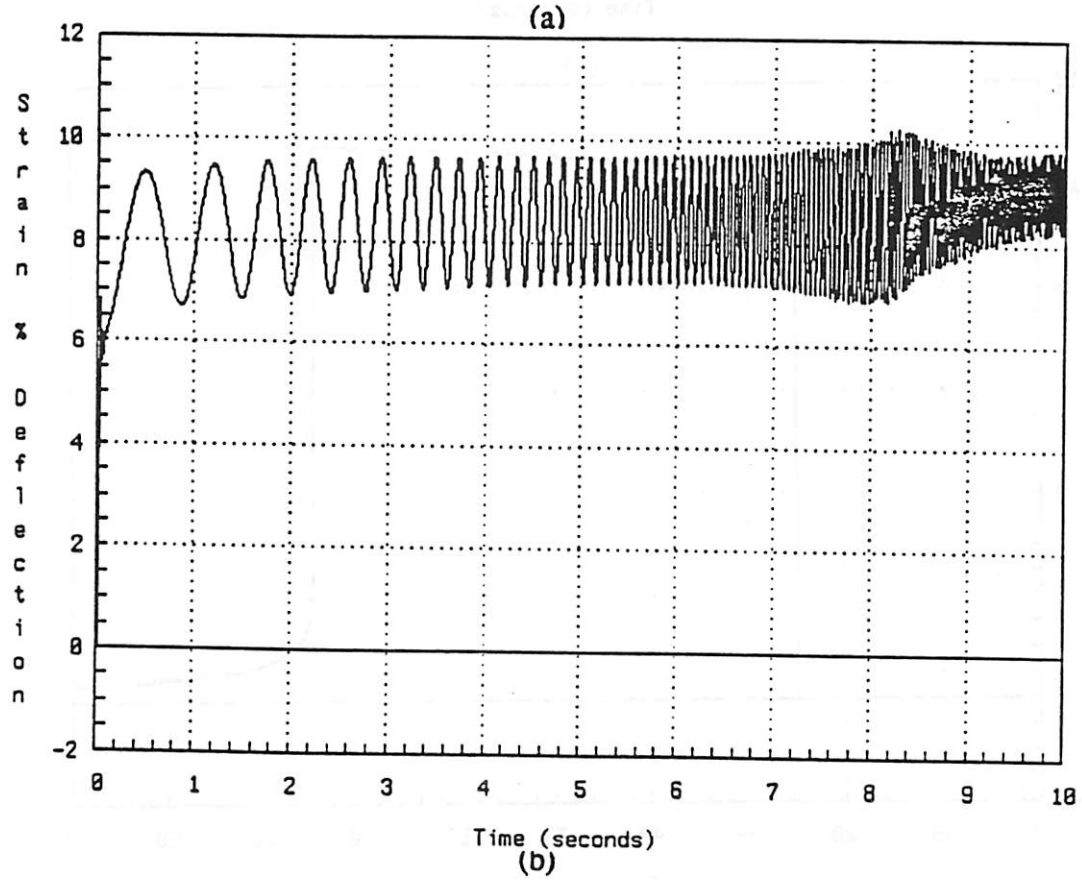

(b)

Graph 3. Response to a sinusoid with exponentially increasing frequency from 1 to 54 Hertz. (a) Input stress expressed as a point force (b) Strain of a tactile element below the point contact

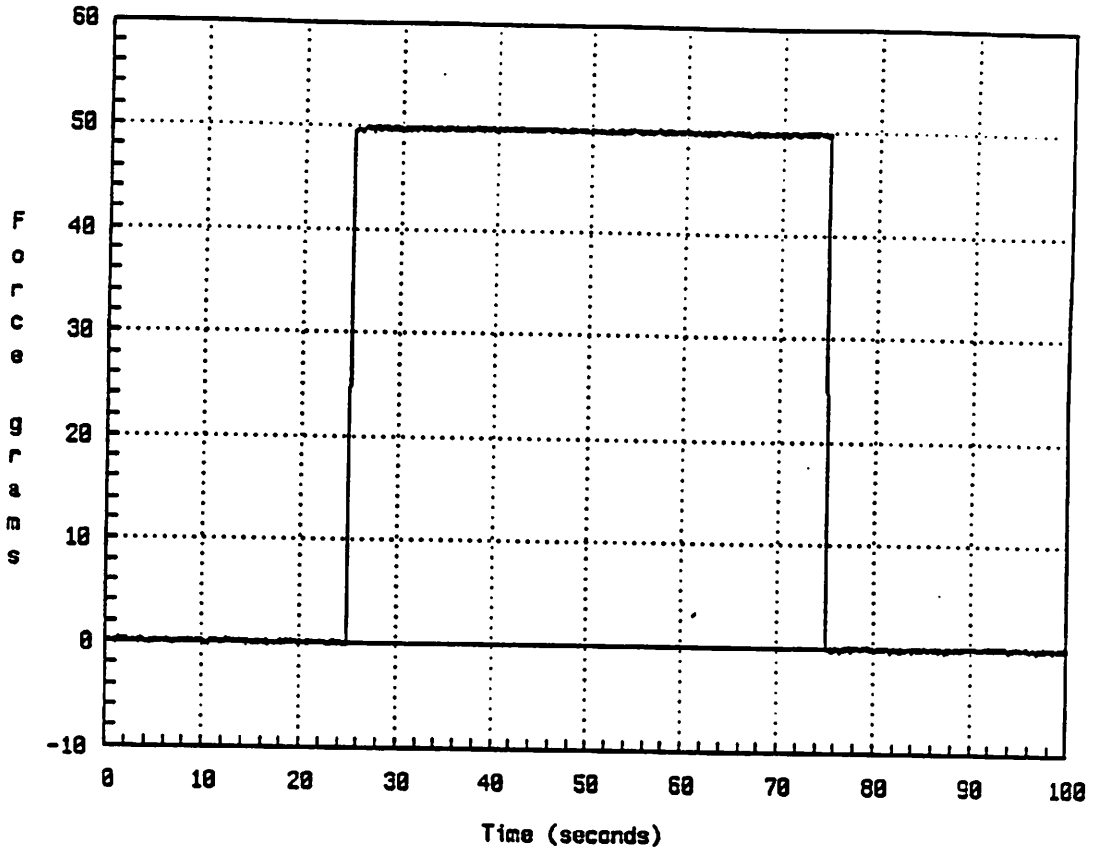

(a)

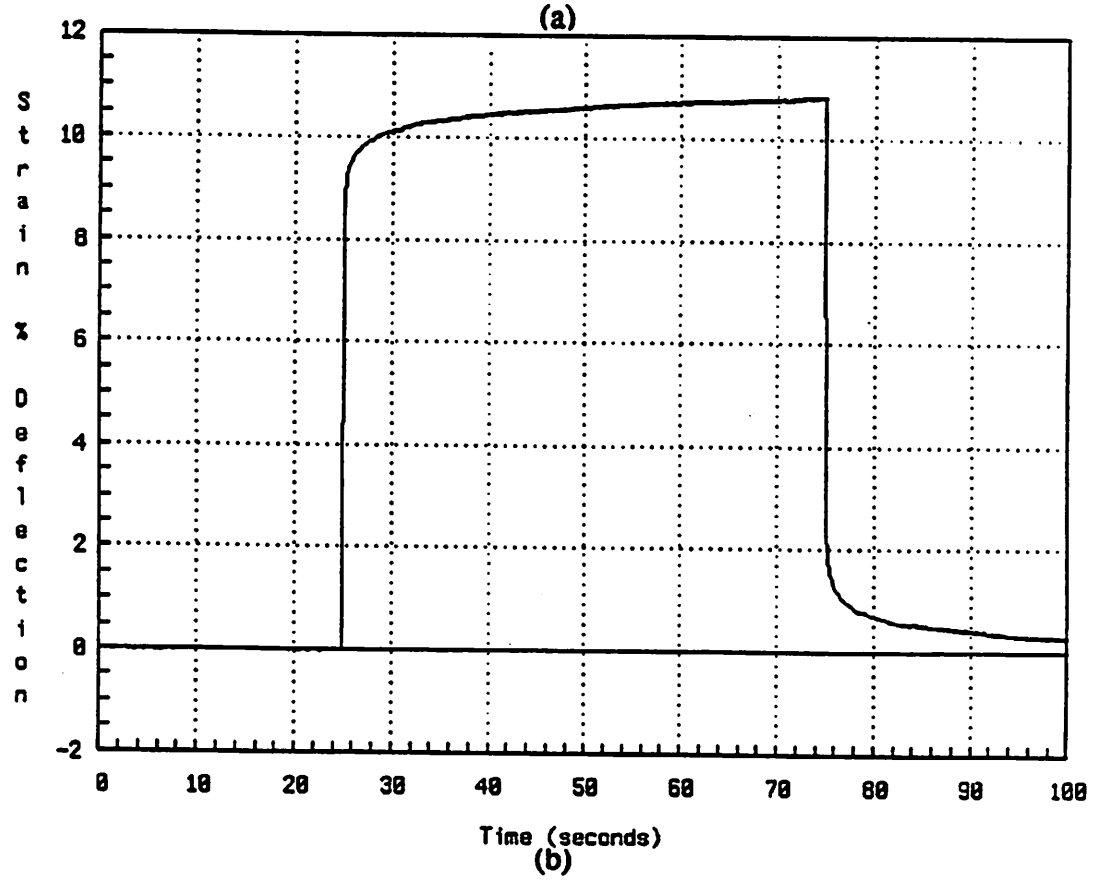

(b)

Graph 4. Step response of the finger, note the initial jump, the exponential increase and the constant drift. (a) load applied (b) finger response.

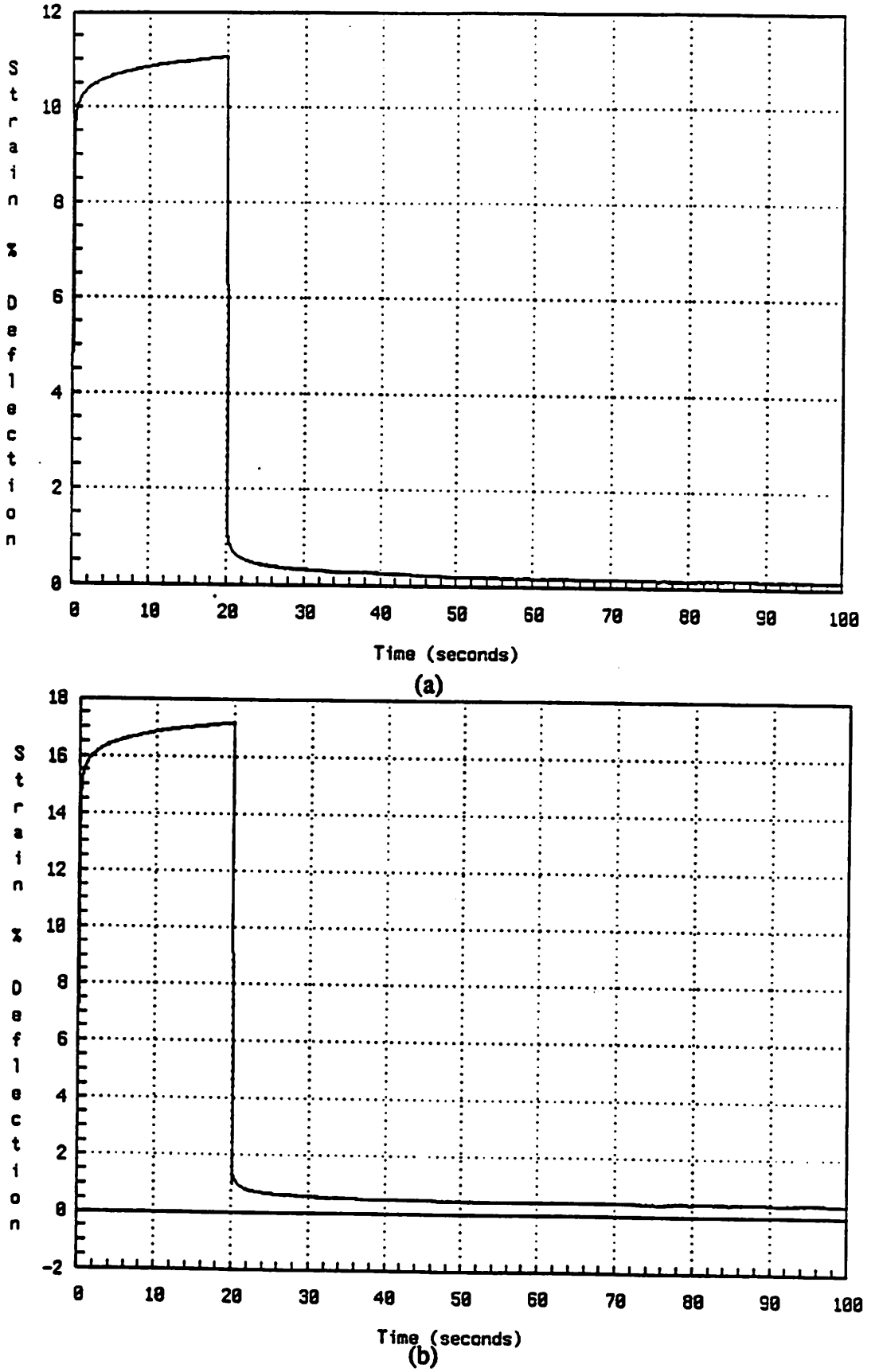

Graph 5. Permanent deformation after 80 seconds of rest. a) 50 gram load, 0.2% deformation b) 100 gram load, 0.4 % deformation

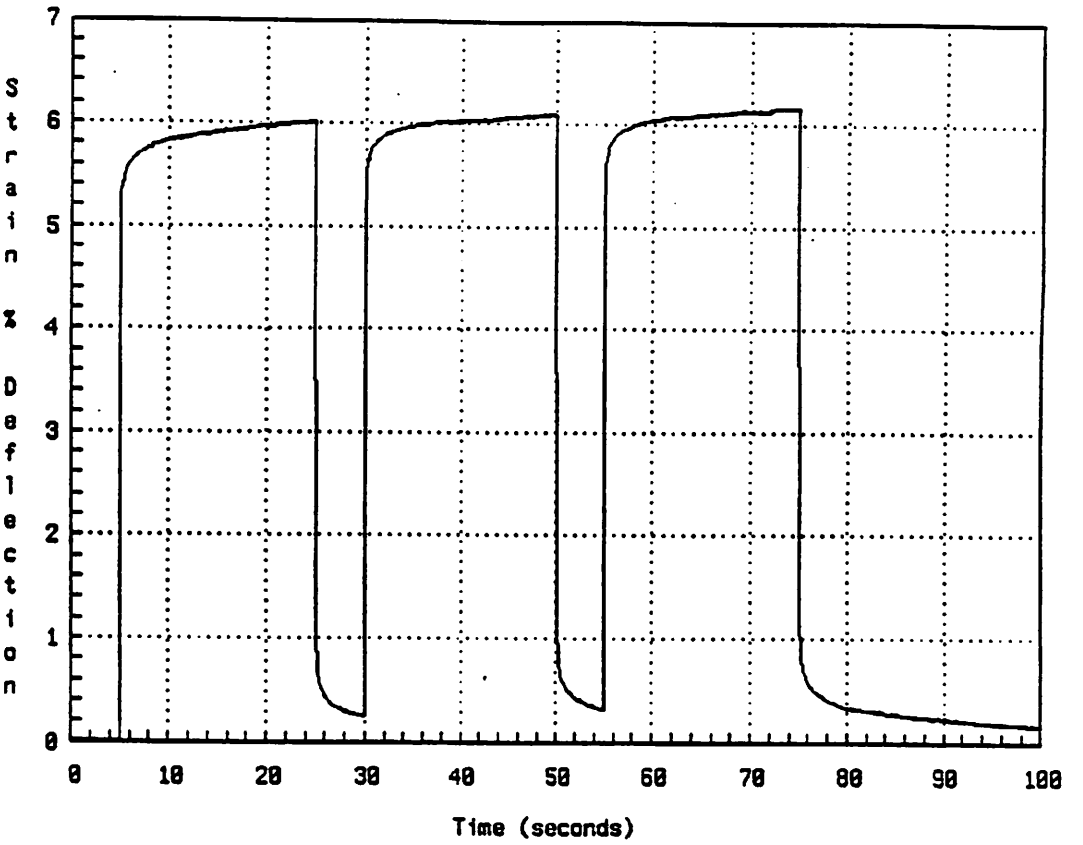

Graph 6. repeated loads, note the decay and the drift

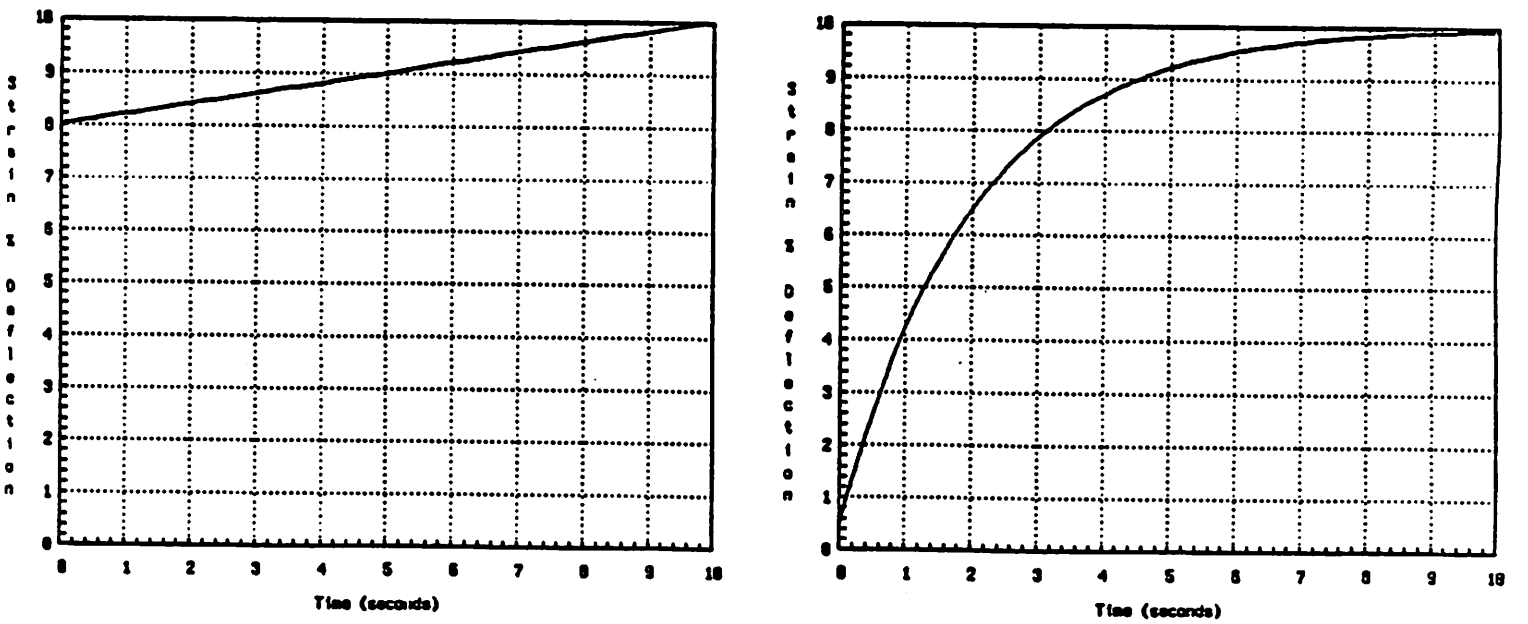

Graph 7. Step Response of a Maxwell Medium, (a), exhibits an initial jump and a constant drift. The step response of a Kelvin medium, (b), is a common delay response

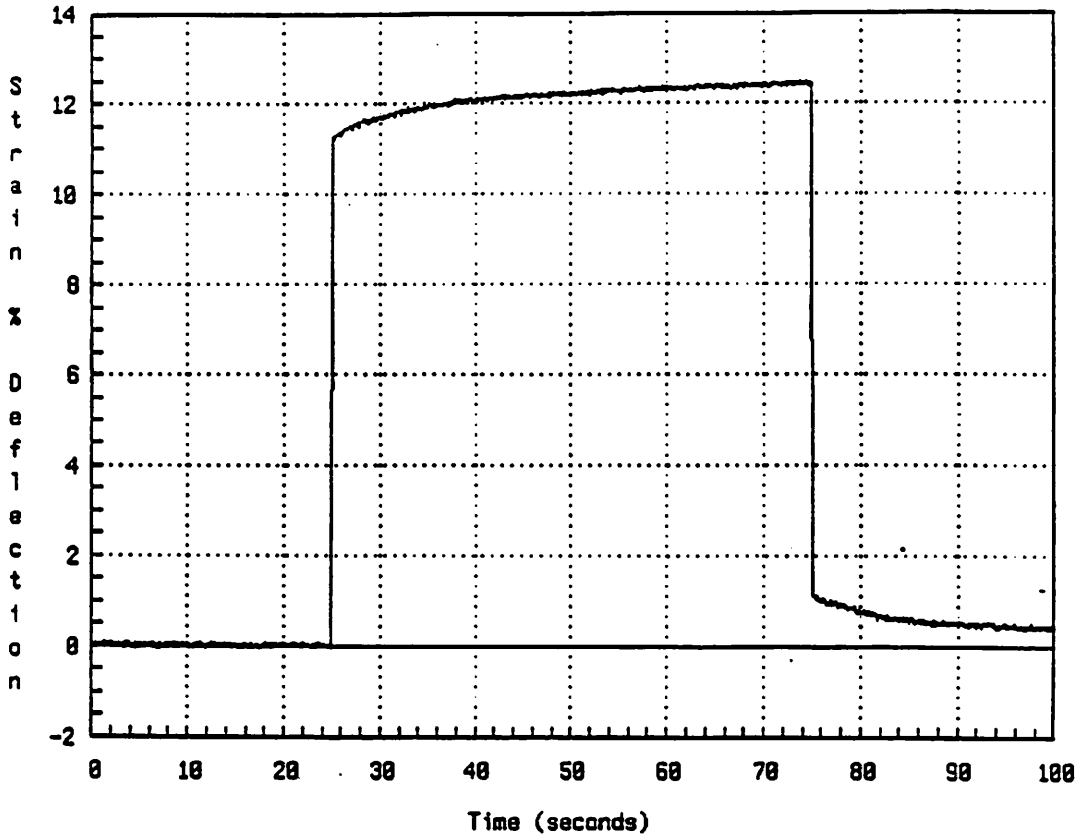

(a)

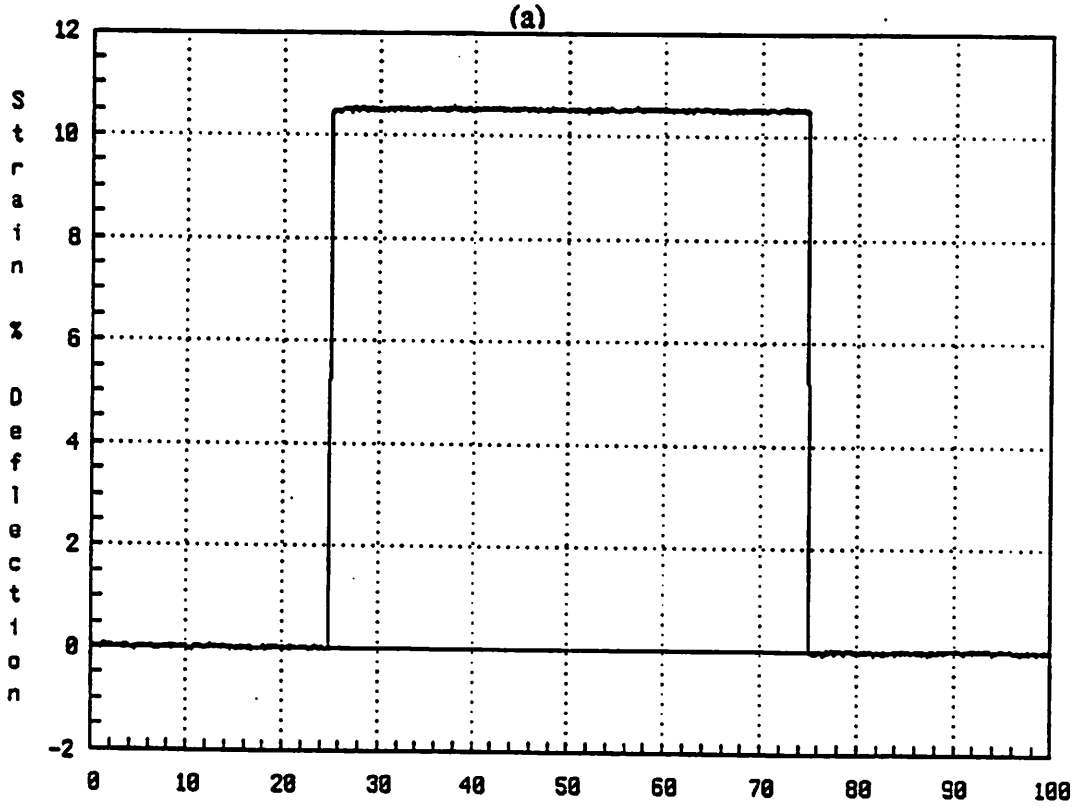

(b)

Graph 8. Simulation of 50 gram step response (a) Maxwell-Kelvin model (b) Elastic model

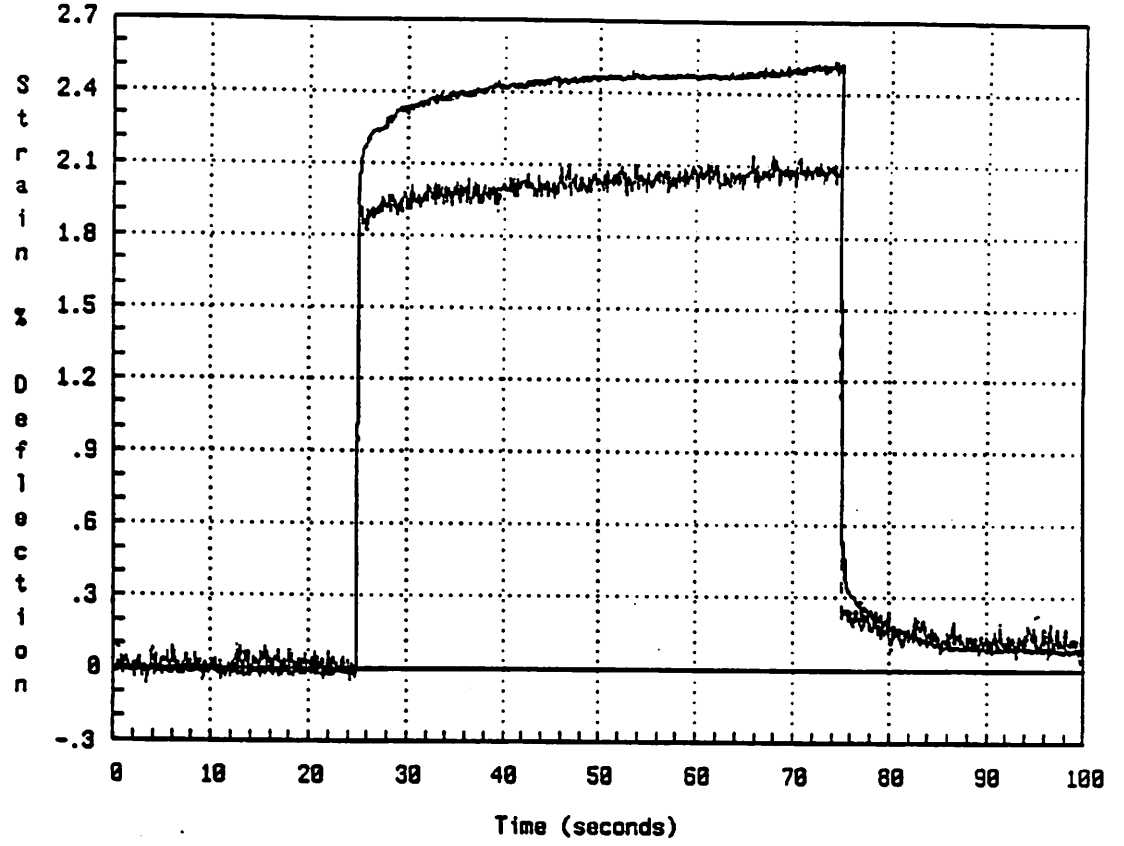

Graph 9. Predicting a 10 gram load response with the response of a model tuned with a 50 gram load.

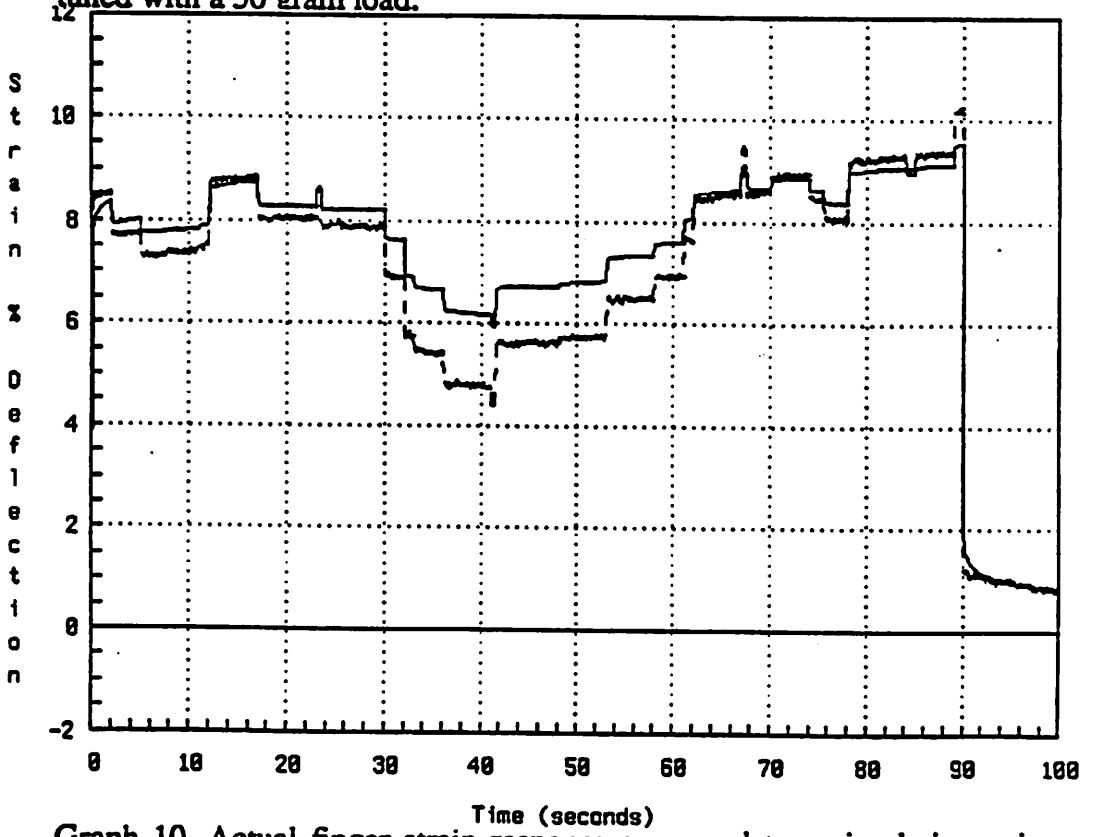

Graph 10. Actual finger strain response compared to a simulation using the Maxwell-Kelvin model tuned with a 30 gram load.

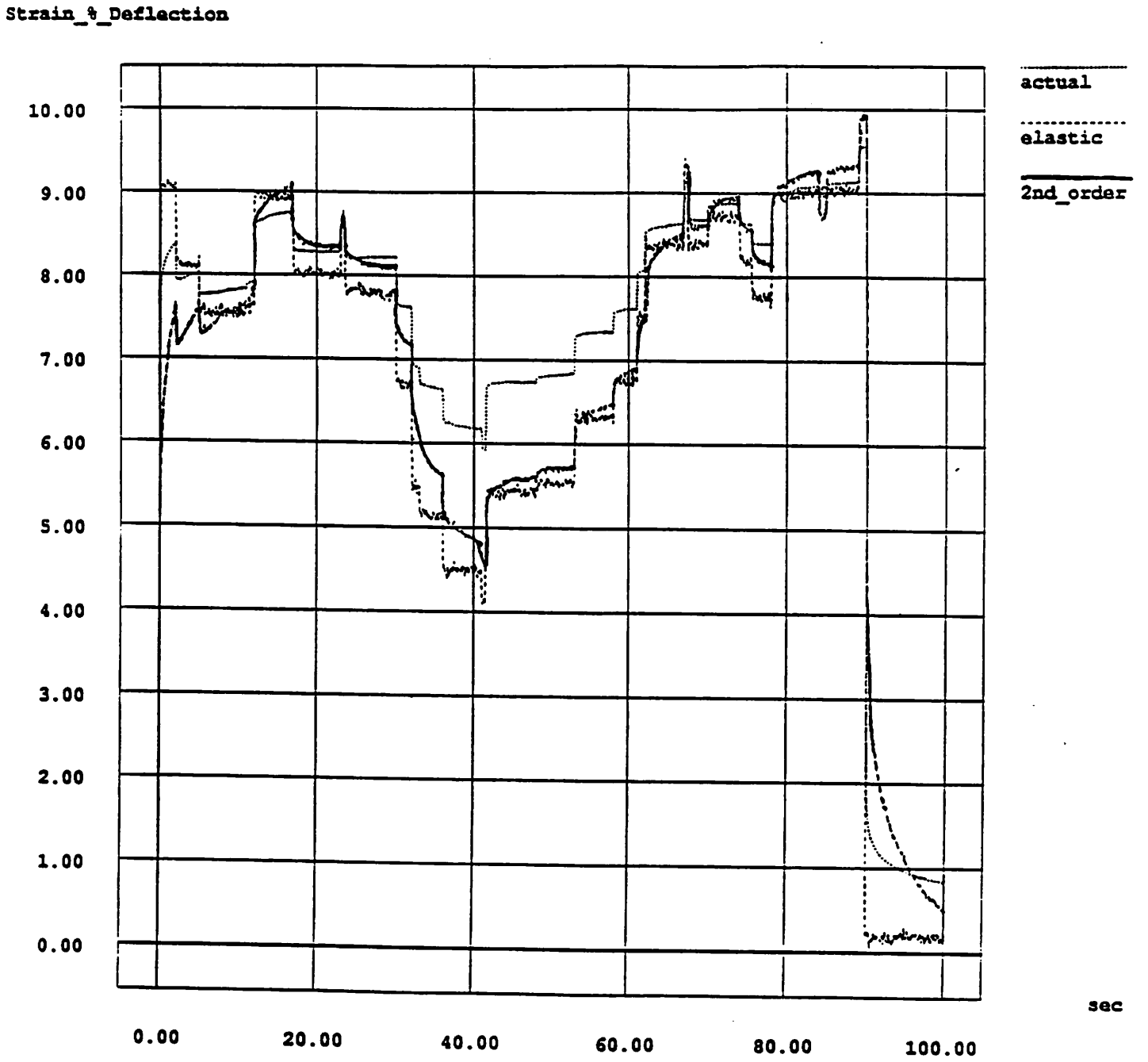

Graph 11. Comparison of actual finger response with elastic model simulation and 2nd order model simulation.

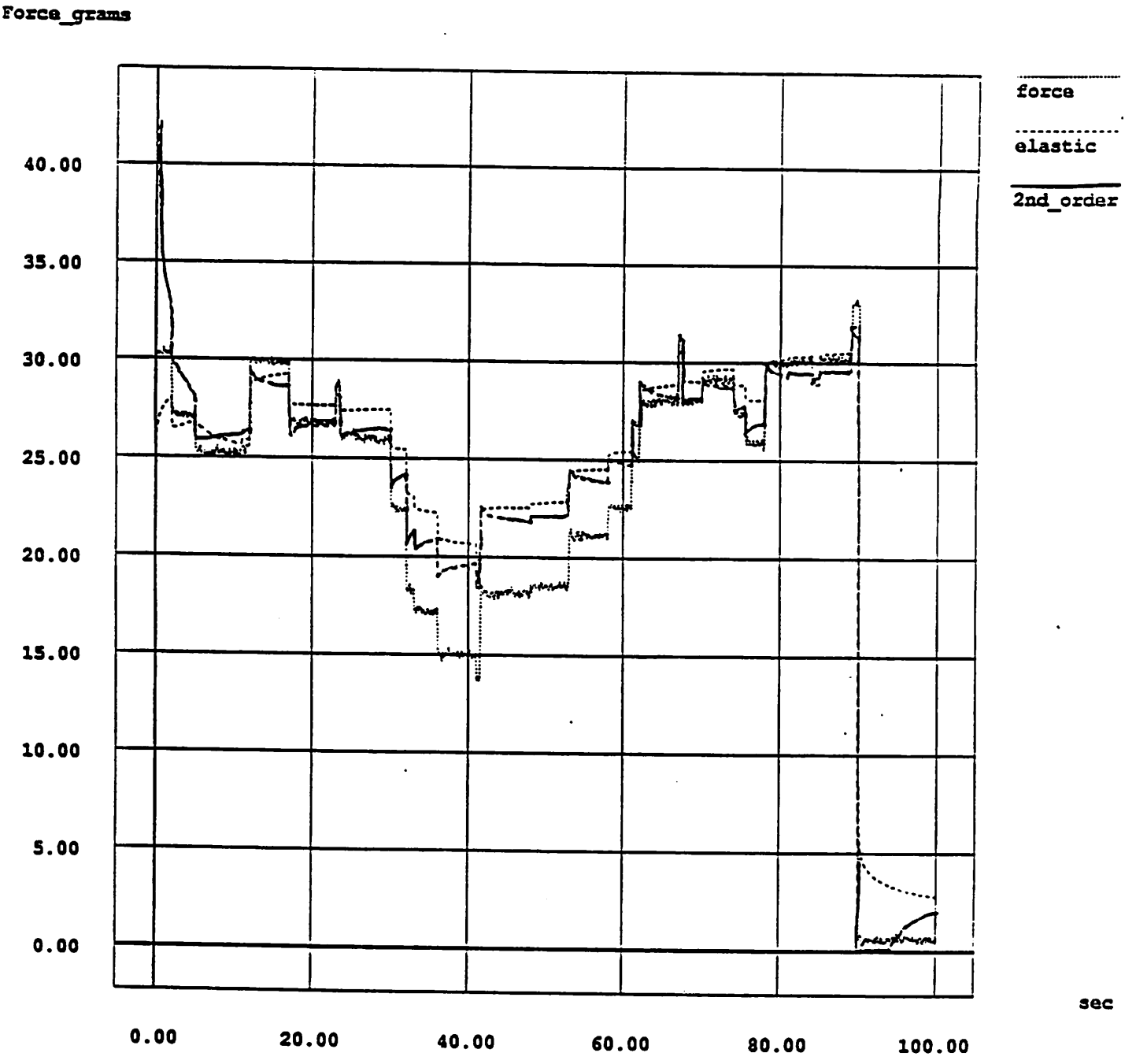

Graph 12. Comparison of actual force with elastic model estimated force and 2nd order model estimated force.

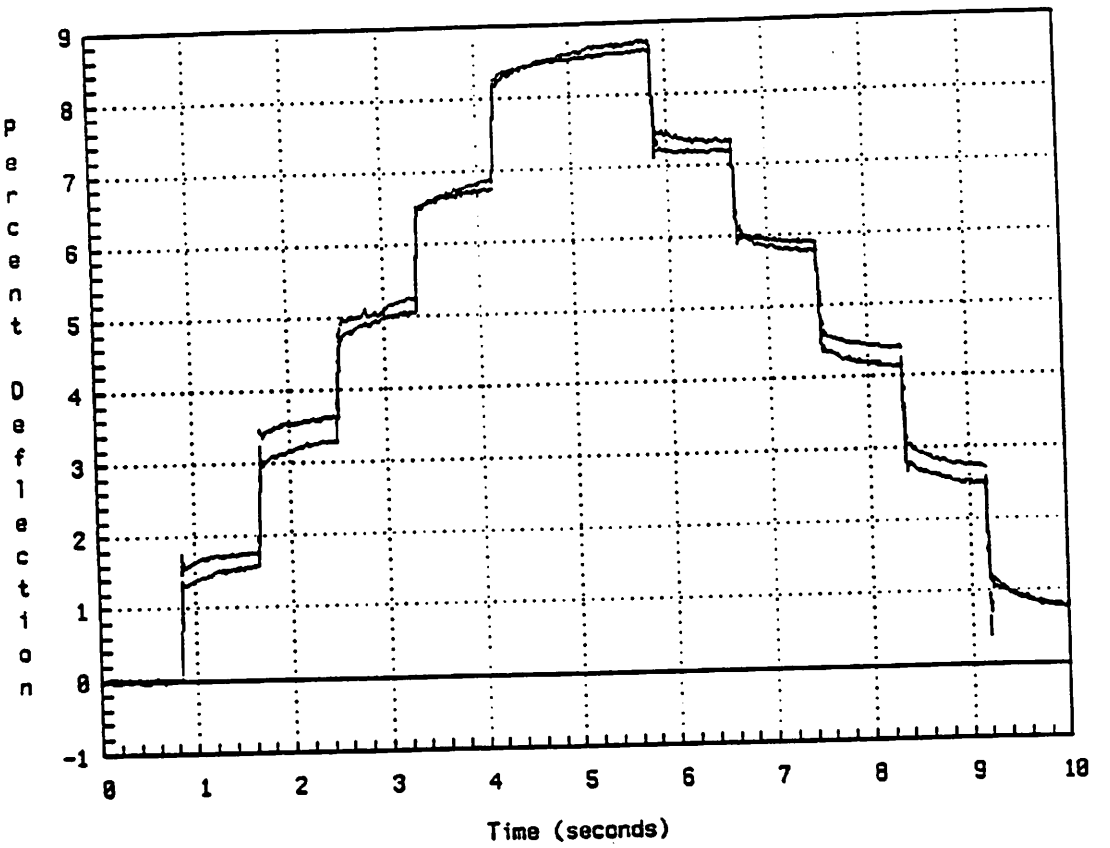

Graph 13. Consecutive step test, second order model response compared to actual finger response.

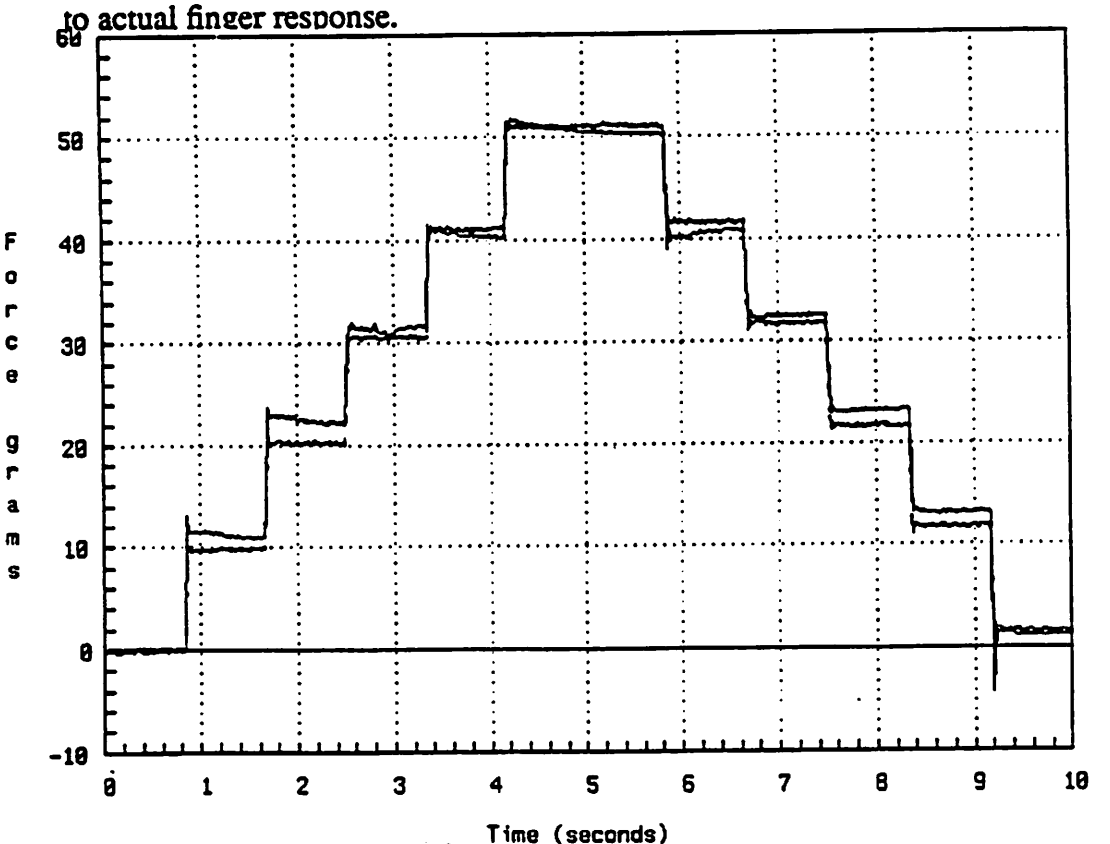

Graph 14. Predicted forces for the consecutive step test

Appendix A: Application of a Small, Observable, Controlled Force

For investigating the force response of the tactile sensor it is necessary to have a force applicator. The design goal was to be able to apply a known and controlled force from zero to 100 grams (100 grams of force = 0.98 Newtons). This was achieved by using a strain gage to sense the applied force, and feeding back the signal to track the desired force input. Figure (a) shows the force response for a command of 10 gram increments (also shown on Graph 14). Figure (b) shows the difference between the commanded force and the force applied for the step increment test. Notice that the error settles to less than a gram after the step commands. The settling time is about 0.08 sec. The (RMS) error of the noise of the strain gage signal is 0.14 grams. Graph 4a shows the actual force applied when a 50 gram step was commanded. The response appears quite accurate since the time between points was 0.1 seconds. The magnitude of frequency response of the force applicator is shown by the sinusoid ramped in frequency displayed in Graph 3a. The response is flat up to about 40 Hz. Near 40 Hz, the response displays a nonlinear effect. Hemispherical and flat contact shapes were used, but experiments with other shapes could be done by simply attaching the desired probe to the end of the force applicator beam.

Figure 1 on page 2 shows the force probe attached to the end of an aluminum beam, which is connected to the shaft of a dc-motor. A strain gage is affixed to the beam. Its signal is amplified by 2100, passed through an A/D converter and used for reading the force applied to the tactile sensor and for feedback control. The motor is powered by a current amplifier that yields 0.19 amps per volt of input. To compensate for the resonant modes of the system a lowpass-notch filter was implemented. The system was digitally controlled by a Motorola 133XT processor board on the "LYMPH" multiprocessor system. The A/D and D/A conversion is done using the hardware via a Data Translation 1407 board. The system block diagram is given in Figure (c).

The system has several features that make control challenging, including: the resonance caused by the motor inertia and springiness of the finger, the lack of viscous friction to aid in damping, the resonant frequencies of the beam, the static friction of the motor, the noisiness of the strain feedback signal, and the probe losing contact with the finger.

A lowpass-notch filter was used to compensate for the inertia-spring resonance of 50 Hz and the beam resonance of 190 Hz, see Figures (d) and (e). This worked well, except that it forced the frequency response of the open loop system to drop off after 20 Hz, see Figure (f). A stiffer beam was not used, since the beam had to be flexible enough

to give a reasonably large strain gage reading. A more sensitive strain gage would allow the use of a stiffer beam which would resonate at a higher frequency. The use of a stiffer beam could alleviate the need for a notch filter as long as a lowpass filter was used. To reduce the inertia-spring resonance, attempts were made to increase the viscous friction. All physical changes to the system to increase the viscous friction also increased the static friction or changed the inertia of the system, yielding unsuccessful results. Furthermore, since the system was quite difficult to model and behaved in a nonlinear fashion, simple PID feedback control did not solve the problem. To avoid the time expense of implementing a more sophisticated control system, the lowpass-notch filter was used.

The static friction problem was overcome by removing the brushes from the motor and soldering wires directly to the commutator. This was successful since the motor only needed to rotate a few degrees. The noise of the strain gage signal was reduced to the value of 0.14 grams RMS error by averaging it 8 times per time interval. The probe losing contact with the finger caused the closed loop proportional-derivative control system to become unstable when small forces (less than 10 grams) were commanded. This problem was alleviated by adjusting the contribution of the feedback gains according to the force command level. For a command of zero grams the feedback gains were zero, and the gains were linearly increased as the command level was increased.

Let:

$f_c(k)$ = commanded force at the kth interval in time,

f_s = force sensed by strain gage,

f_a = adjusted command (is converted to analog voltage and applied to notch filter),

$e(k+1)$ = command error = $f_c(k+1) - f_s(k)$,

K_d = derivative control gain = 0.03,

K_p = proportional control gain = 2.0,

K_e = error control gain = 1.0,

Δt = 0.001 seconds,

then the control law is given by,

$$f_a(k+1) = f_c(k+1) + (K_e f_c(k+1)/100)\,(K_p\, e(k+1) + K_d\, \frac{e(k+1) - e(k)}{\Delta t}) \qquad \text{(A1)}$$

The following pages give the technical details of the force applicator device.

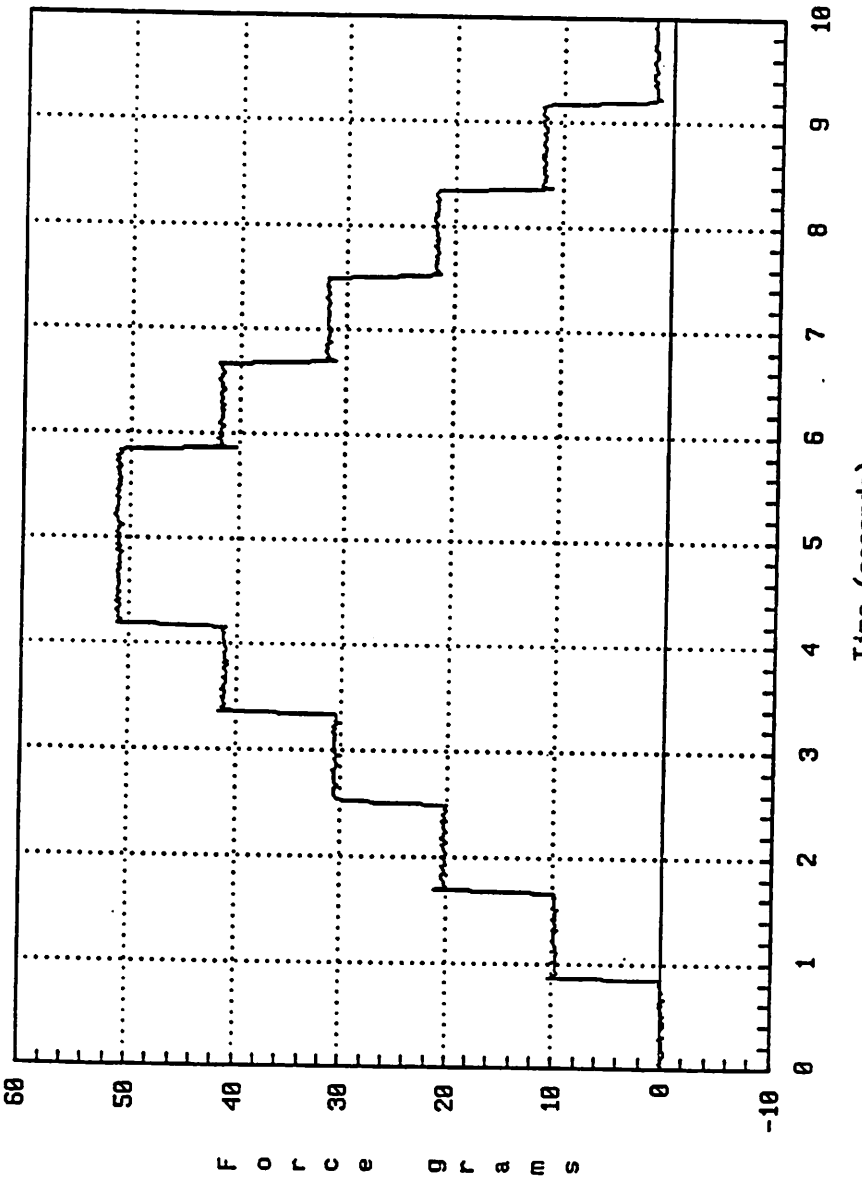

Figure (a) Force applied to finger as sensed by the strain gage, the reference input was 10 gram steps at 1/12 second intervals.

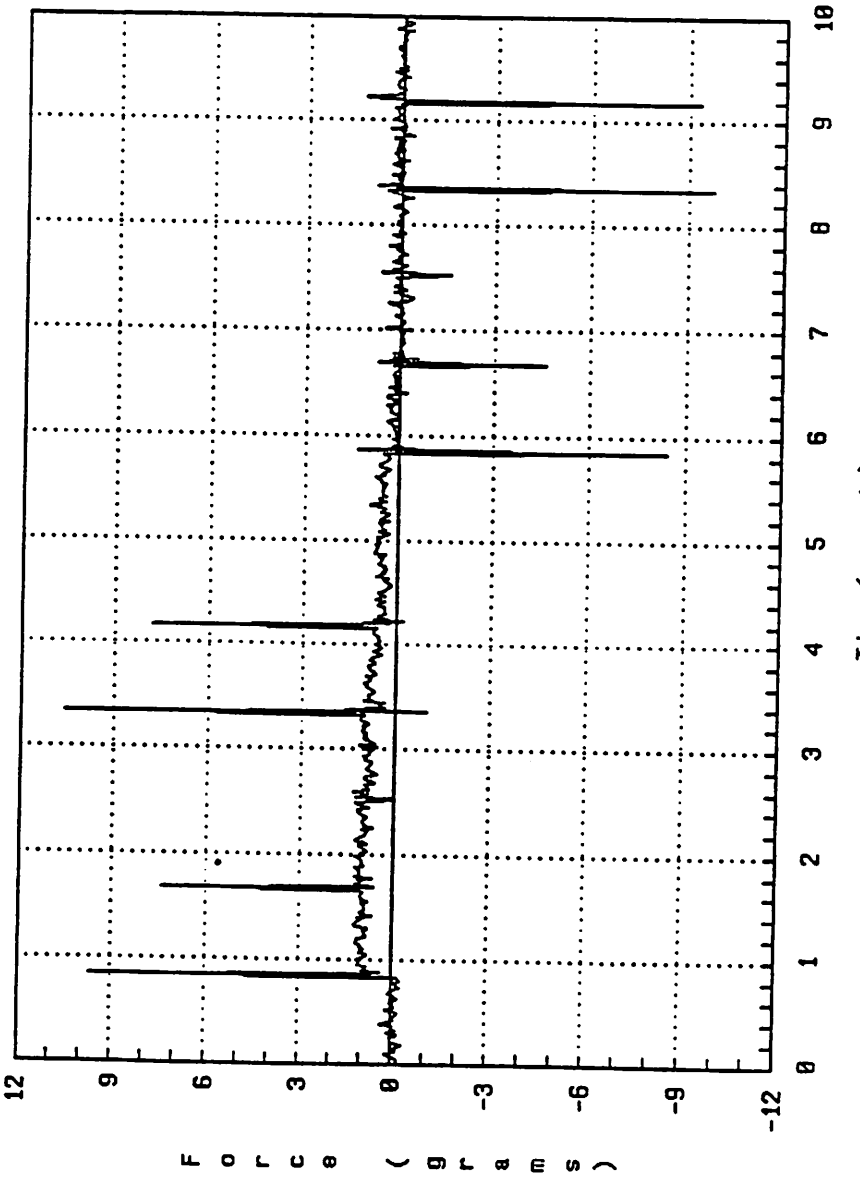

Figure (b) Difference between reference input and sensed force for the experiment shown in Figure (a).

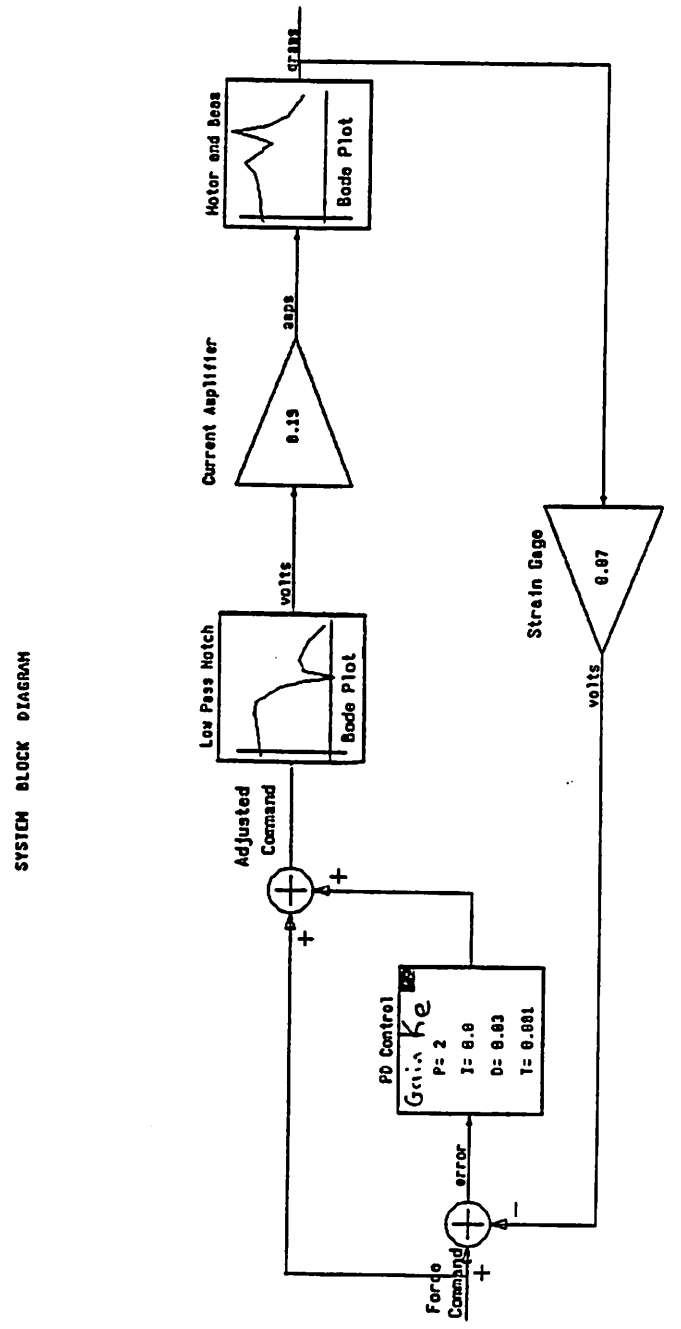

Figure (c) System Block Diagram. Note the use of strain gage feedback and lowpass-notch filter to improve control.

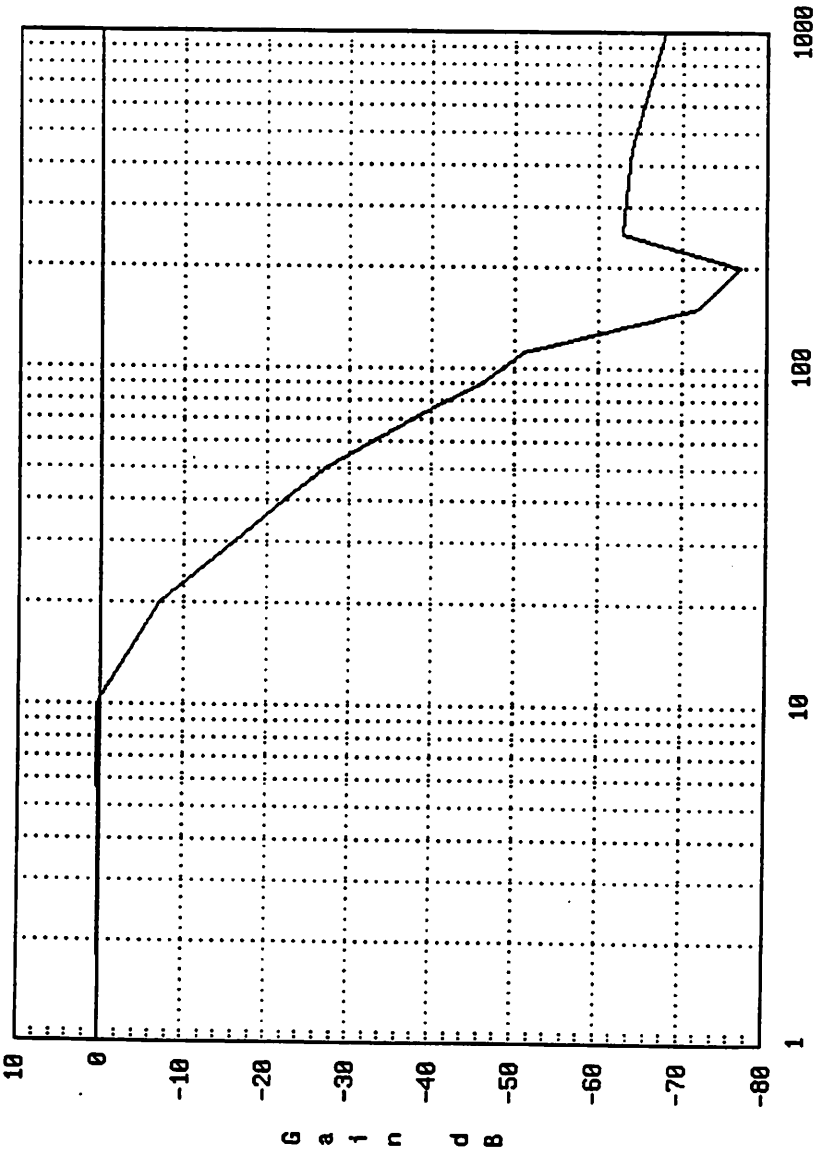

Figure (d) Notch Filter Response

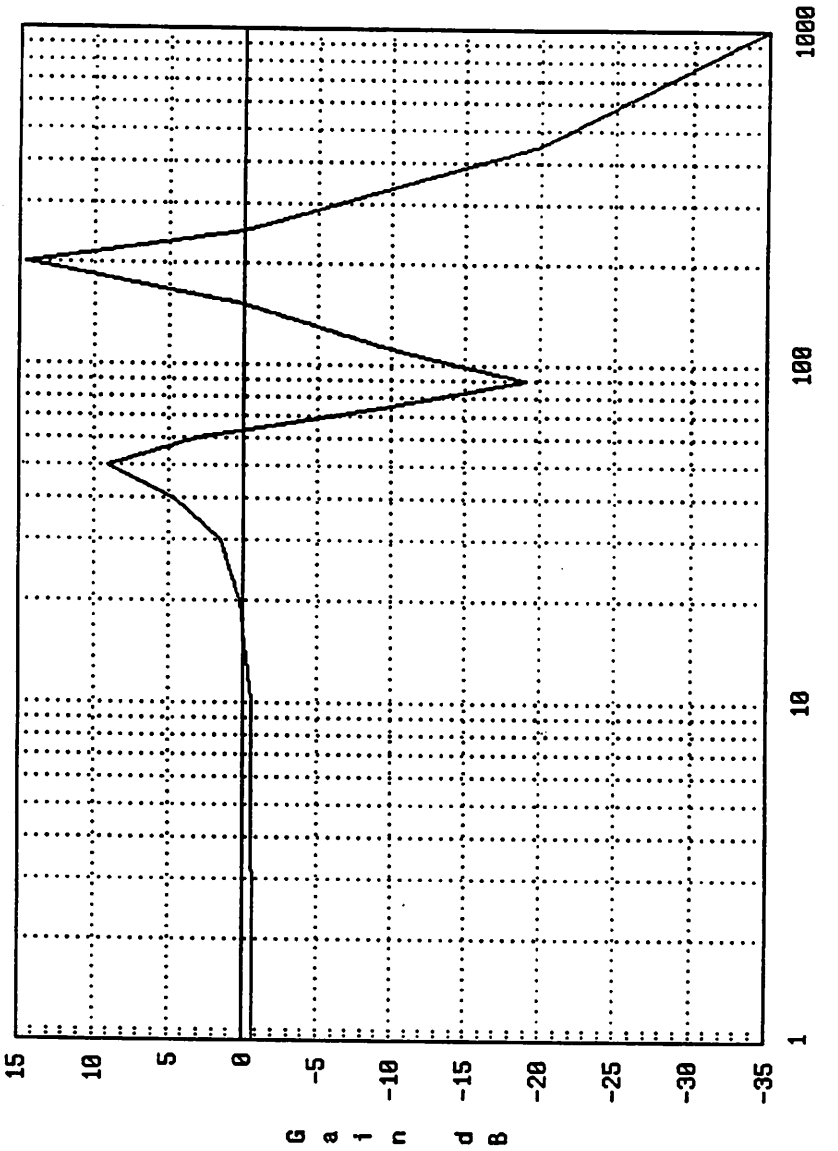

Figure (e) Motor-Beam Response

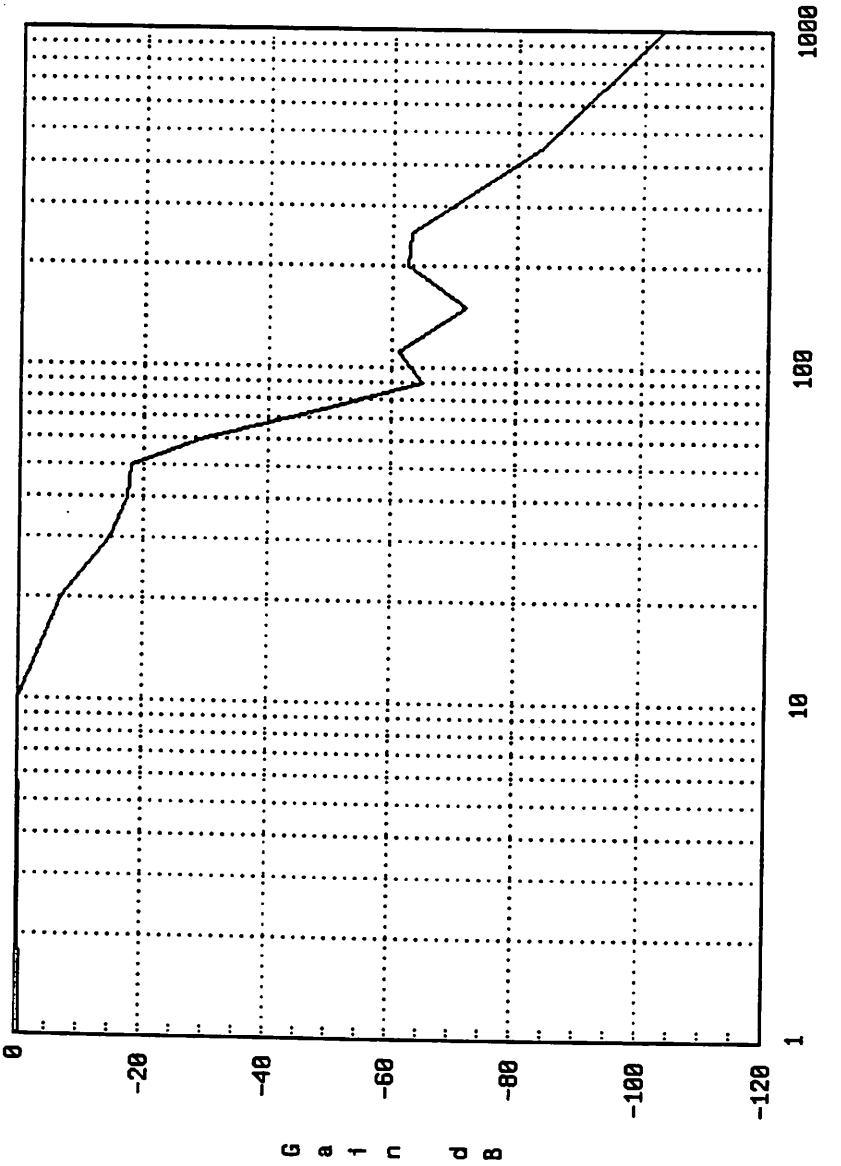

Figure (f) Open Loop Response

Current Amplifier*

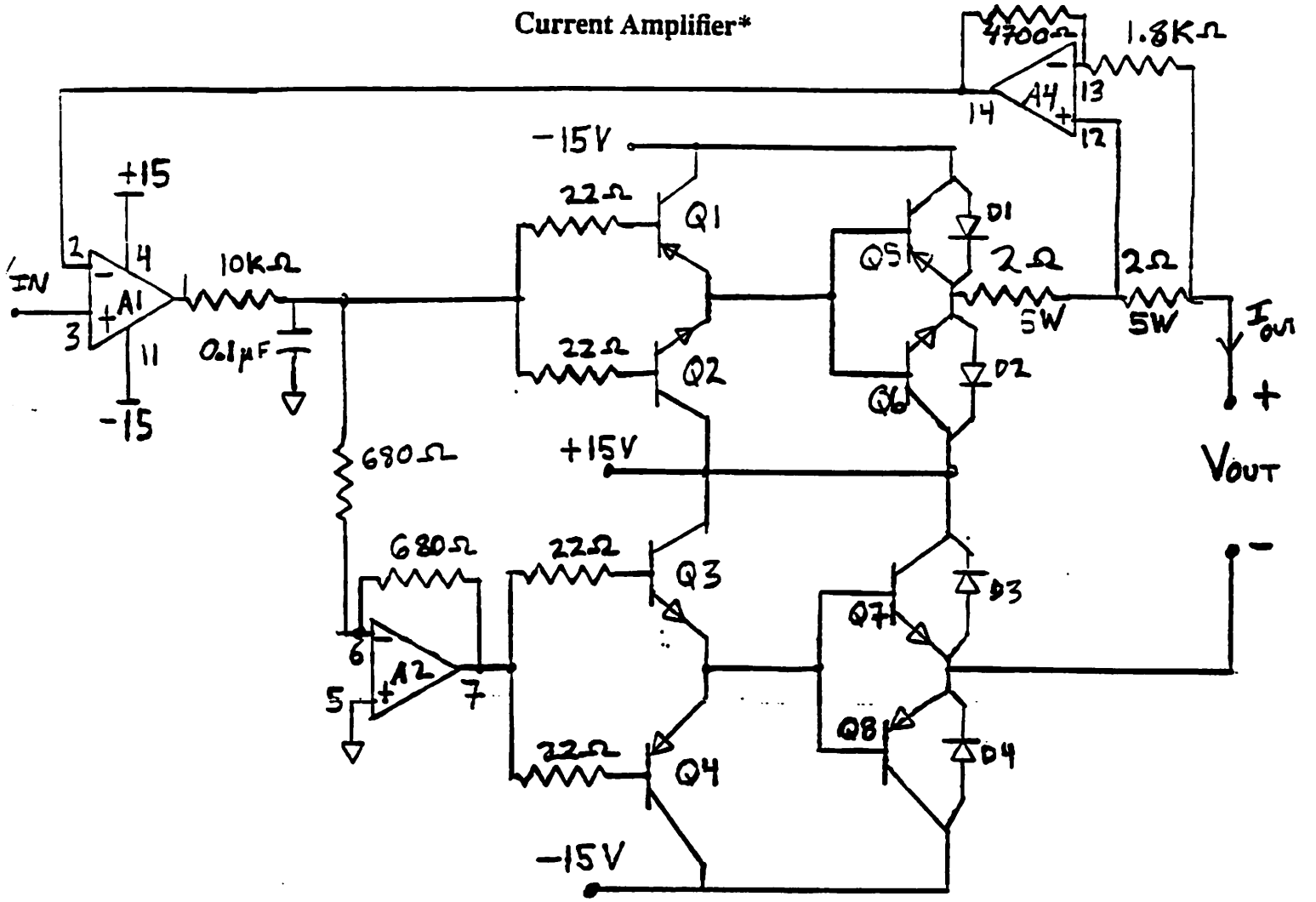

Gain: I_{out}/V_{in} = 0.19 amps/volt 3dB point: 160 Hz

Power Supply: POWER-ONE International Series HCC15-3-A +/- 15 volts 3 amps

Circuit Elements:

A1, A2, A4:	Quad-Op-Amp	TL704CN
Q1, Q4:	PNP	2N2905
Q2, Q3:	NPN	2N2219
Q5, Q8:	PNP	2N6247
Q6, Q7:	NPN	2N6472
D1,D2,D3,D4:	Diode	1N4004

* Circuit Design is a modification of one developed by Raja Kadiyala, Robotics Lab, EECS Dept., University of California, Berkeley.

Low Pass Notch Filter*

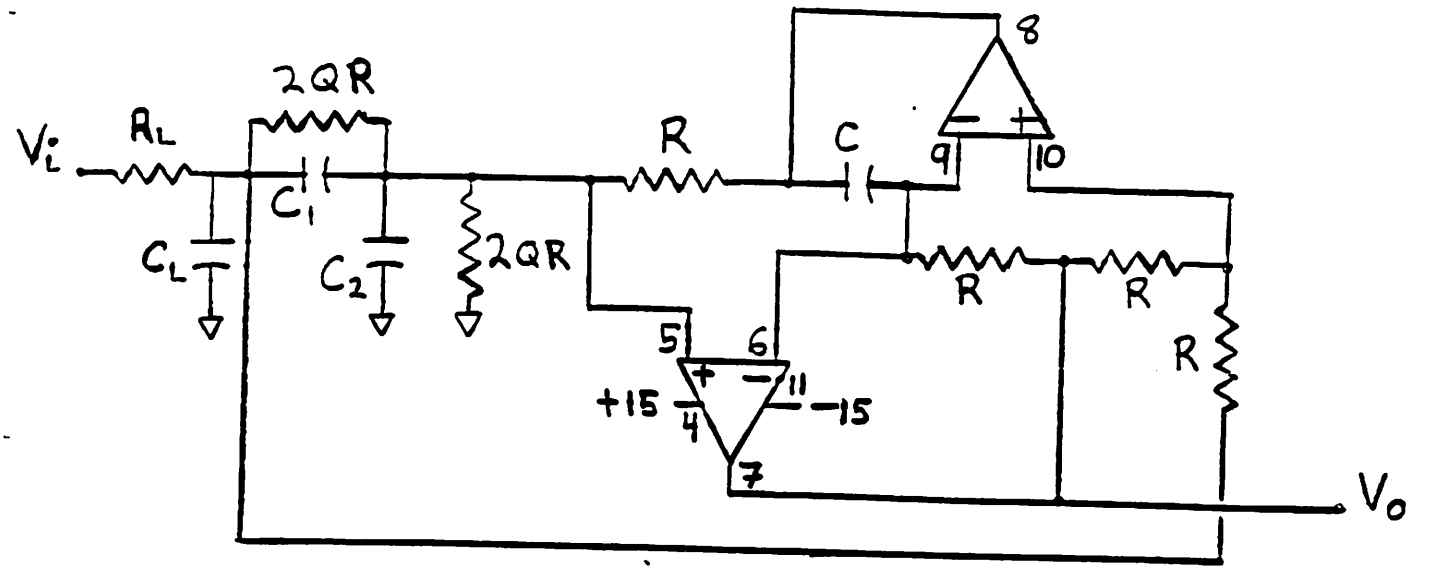

Transfer Function:

$$\frac{V_o(s)}{V_i(s)} = \left[\frac{1}{s/\omega_l + 1}\right] \frac{\left[\frac{\omega_o}{\omega_n}\right]^2 (s^2 + \omega_n{}^2)}{s^2 + \frac{\omega_o}{Q} s + \omega_o{}^2}$$

Component Values Determine the Pole and Zero Frequencies:

$R_l = 6800\,\Omega$, $C_l = 1\,\mu F \implies \omega_l = 147\ rad/sec$, $f_l = 23.4\ Hz$

$R = 2.7\,k\Omega$, $C = 2.2\,\mu F \implies \omega_o = 168\ rad/sec$, $f_o = 26.8\ Hz$

$\alpha = \omega_n/\omega_o$

$$C_1 = \left[\frac{1}{2} + \frac{1}{2\alpha^2}\right] C \qquad C_2 = \left[\frac{1}{2} - \frac{1}{2\alpha^2}\right] C$$

$C_1 = 1.13\,\mu F \implies \alpha = 6.6$, $C_2 = 1.08\,\mu F \implies \alpha = 7.4 \implies \omega_n = 190\ Hz$

$Q = 2.8 \implies 2QR = 15\,k\Omega$

* Circuit from Ghausi and Laker (1981), page 217.

Motor and Strain Gage Data

Motor: Electro-Craft Model: E-586

Torque Constant: 12.6 *oz–in/amp* = 910 *gram–cm/amp*
Armature Inertia: 0.0053 $oz–in–sec^2$ = 0.38 $gram–cm–sec^2$
Static Friction No Brushes: ≈ 10 *gram–cm*
Damping Factor: 0.1 *oz–in/KRPM* = 432 *gram–in/(deg/sec)*
Armature Resistance: 2.0 Ω
Armature Inductance: 4.9 *mH*

Note: the brushes were removed and wires were soldered directly onto the commutator.

Strain Gage: Measurements Group

Bridge voltage: 10 *volts*
Amplifier Gain: 2100
Ratio of force at end of beam to amplifier voltage: 14 *grams/volt*
Standard Deviation of noise of strain gage signal at A/D converter: 0.1 volts

Moment Arm Length: 9 *cm*

Finger Amplifier Circuit

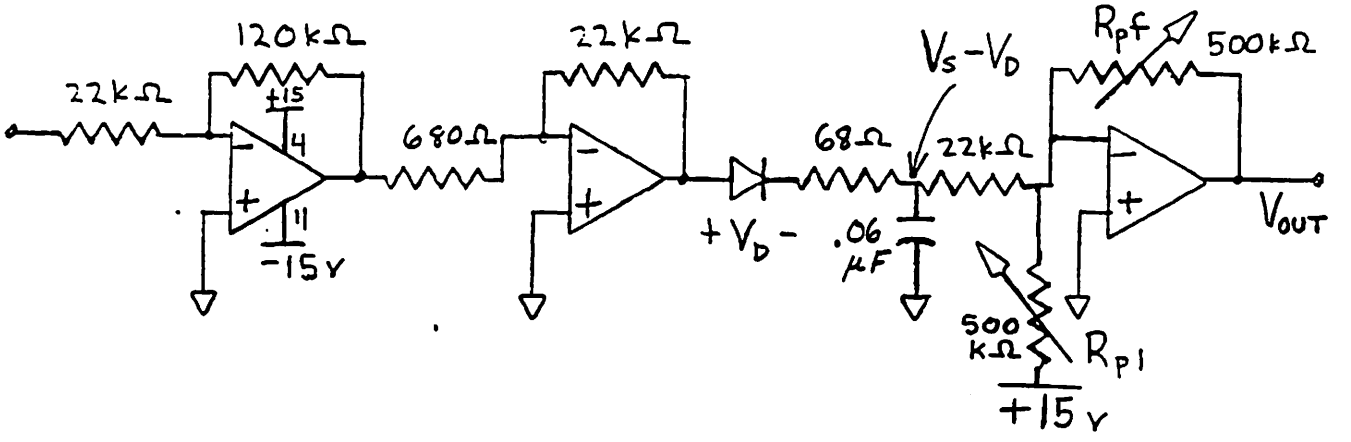

V_s = amplified magnitude of the sinusiodal sensed voltage signal from a tactile element (≈ 5 volts).
V_o = amplified magnitude of the sinusoidal voltage across a tactile element when there is no deflection.
V_D = voltage drop across the diode = 0.6 volts.
V_{out} = voltage read by A/D converter
V_{cc} = positive power supply voltage = 14.7 volts
R_{pf} = potentiometer = 187 $k\Omega$ (for element 4,2: the 4th ring from the base, 2nd axial strip).
R_{p1} = potentiometer = 48 $k\Omega$ (for element 4,2)

The circuit has three stages: pre-amplification, envelop detection, and final offset and amplification. The first stage amplifies the 200 kHz signal to overcome the voltage drop across the diode. The diode and single pole low pass filter acts as an envelop detector. The final stage allows the user to set the offset close to zero and adjust the final output voltage range by adjusting the potentiometers R_{p1} and R_{pf}. This final adjustment assures that the output voltage range will be within the +/- 10 volt range of the A/D converter. that it can be read by the A/D converter.

The goal is to recover strain in percentage deflection from V_{out}. The voltage after the envelop detector is $V_s - V_D$, and from equation (6) on page 6, we need $(V_s - V_o)/V_o$. When there is no strain:

$$V_{outo} = -R_{pf}\left[\frac{V_{cc}}{R_{p1}} + \frac{V_o - V_D}{22k}\right]$$

and when there is an arbitrary amount of strain:

$$V_{outs} = -R_{pf}\left[\frac{V_{cc}}{R_{p1}} + \frac{V_s - V_D}{22k}\right]$$

$$V_{outs} - V_{outo} = -\frac{R_{pf}}{R_1}(V_s - V_o)$$

$$V_o = -\frac{R_1}{R_{pf}}\left[V_{outo} + \frac{R_{pf}}{R_{p1}}(V_{cc})\right] + V_D$$

Using the above relation for V_o, the strain, ε, of the tactile element can be written in terms of measurable voltages and known constants. The units are percentage deflection.

$$\varepsilon = \frac{V_s - V_o}{V_o} = \frac{-\frac{R_1}{R_{pf}}(V_{outs} - V_{outo})}{V_o}$$